12-4-2023

Mitochondrial GTP metabolism controls reproductive aging in C. elegans

Yi-Tang Lee
Baylor College of Medicine

Marzia Savini
Baylor College of Medicine

Tao Chen
Howard Hughes Medical Institute

Yang, Jin
University of Wisconsin - Madison

Qian Zhao
Howard Hughes Medical Institute

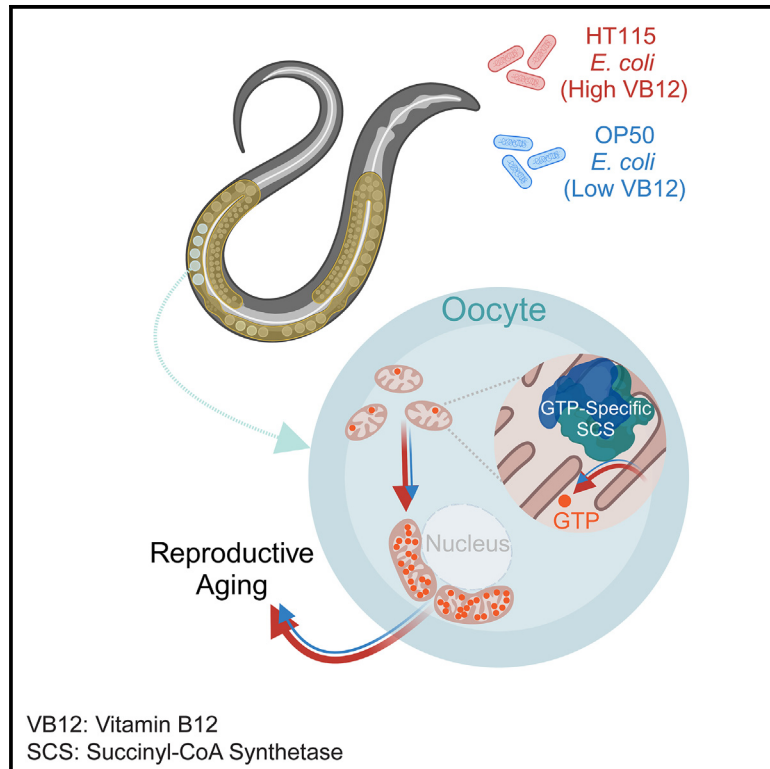*See next page for additional authors*

Recommended Citation

Authors

Yi-Tang Lee; Marzia Savini; Tao Chen; Yang, Jin; Qian Zhao; Lang Ding; Shihong Max Gao; Jessica N. Sowa; Jue D. Wang; and Meng C. Wang

Mitochondrial GTP metabolism controls reproductive aging in *C. elegans*

Graphical abstract

VB12: Vitamin B12
SCS: Succinyl-CoA Synthetase

Authors

Yi-Tang Lee, Marzia Savini,
Tao Chen, ..., Jessica N. Sowa,
Jue D. Wang, Meng C. Wang

Correspondence

mengwang@janelia.hhmi.org

In brief

Lee et al. identify a signaling nexus between mitochondrial GTP metabolism and mitochondrial dynamics in regulating *C. elegans* reproductive aging. They further demonstrate that bacterial metabolites act through this signaling mechanism to modulate the host's reproductive health during aging.

Highlights

- Mitochondrial GTP-specific succinyl-CoA synthetase regulates reproductive longevity

- Oocyte mitochondrial positioning influences reproductive health during aging

- Mitochondrial fission in the oocyte promotes reproductive longevity

- Bacterial vitamin B12 modulates reproductive aging via GTP succinyl-CoA synthetase

CellPress

Article

Mitochondrial GTP metabolism controls reproductive aging in *C. elegans*

Yi-Tang Lee,[1,2] Marzia Savini,[2,3] Tao Chen,[4] Jin Yang,[5] Qian Zhao,[4] Lang Ding,[4,6] Shihong Max Gao,[3,4] Mumine Senturk,[2,7] Jessica N. Sowa,[8] Jue D. Wang,[5] and Meng C. Wang[4,7,9,*]

[1]Integrative Program of Molecular and Biochemical Sciences, Baylor College of Medicine, Houston, TX 77030, USA
[2]Huffington Center on Aging, Baylor College of Medicine, Houston, TX 77030, USA
[3]Graduate Program in Developmental Biology, Baylor College of Medicine, Houston, TX 77030, USA
[4]Howard Hughes Medical Institute, Janelia Research Campus, Ashburn, VA 20147, USA
[5]Department of Bacteriology, University of Wisconsin-Madison, Madison, WI 53706, USA
[6]Graduate Program in Chemical, Physical & Structural Biology, Graduate School of Biomedical Science, Baylor College of Medicine, Houston, TX 77030, USA
[7]Howard Hughes Medical Institute, Baylor College of Medicine, Houston, TX 77030, USA
[8]Department of Biology, West Chester University, West Chester, PA 19383, USA
[9]Lead contact
*Correspondence: mengwang@janelia.hhmi.org
https://doi.org/10.1016/j.devcel.2023.08.019

SUMMARY

Healthy mitochondria are critical for reproduction. During aging, both reproductive fitness and mitochondrial homeostasis decline. Mitochondrial metabolism and dynamics are key factors in supporting mitochondrial homeostasis. However, how they are coupled to control reproductive health remains unclear. We report that mitochondrial GTP (mtGTP) metabolism acts through mitochondrial dynamics factors to regulate reproductive aging. We discovered that germline-only inactivation of GTP- but not ATP-specific succinyl-CoA synthetase (SCS) promotes reproductive longevity in *Caenorhabditis elegans*. We further identified an age-associated increase in mitochondrial clustering surrounding oocyte nuclei, which is attenuated by GTP-specific SCS inactivation. Germline-only induction of mitochondrial fission factors sufficiently promotes mitochondrial dispersion and reproductive longevity. Moreover, we discovered that bacterial inputs affect mtGTP levels and dynamics factors to modulate reproductive aging. These results demonstrate the significance of mtGTP metabolism in regulating oocyte mitochondrial homeostasis and reproductive longevity and identify mitochondrial fission induction as an effective strategy to improve reproductive health.

INTRODUCTION

As one of the earliest signs of age-associated decline, reproductive senescence has a strong impact on society due to the trend of increased average maternal age at first birth.[1] Aged women exhibit decreased fertility and increased rates of birth defects and miscarriages.[2] It is estimated that fertility decline occurs on an average of 10 years prior to menopause, and an age-associated decrease in oocyte quality is the major cause for this decline.[3] Diverse factors can influence oocyte quality, and one of the main contributors is mitochondrial activity.[4] Oocytes have the largest number of mitochondria among all the cells in an organism.[5] Changes in mitochondrial adenosine triphosphate (ATP) production, membrane potential, and DNA copy numbers have been reported to influence oocyte development, maturation, and fertility.[4,6–8] Meanwhile, mitochondria exhibit highly dynamic morphology and constantly undergo organellar fission and fusion, leading to changes in their shape, size, and distri-

bution.[9] Specific types of protein machinery are required to maintain mitochondrial fission-fusion dynamics, including the mitochondrial fission guanosine triphosphatase (GTPase) dynamin-related protein 1 (DRP1), mitochondrial outer membrane fusion GTPases MitoFusiN 1 (MFN1) and MFN2, and mitochondrial inner membrane fusion GTPase optic atrophy 1 (OPA1).[9] These regulators of mitochondrial dynamics also modulate mitochondrial distribution within the cell, especially in the oocyte. In mice with Drp1 knockout (KO), the oocyte mitochondrial network is aggregated toward the perinuclear region.[10] Similarly, in mouse oocytes overexpressing Mfn1 or Mfn2, the mitochondrial network exhibits perinuclear accumulation without increasing tubular elongation.[11] Mitochondrial fission-fusion factors have also been linked with oocyte development and maturation.[10,12,13] Drp1 KO in mice oocytes results in abnormal follicular maturation and fertility decline.[10] Oocyte-specific KO of mouse Mfn1 causes defective folliculogenesis, apoptotic cell loss, and complete infertility.[12,13] These findings indicate the importance
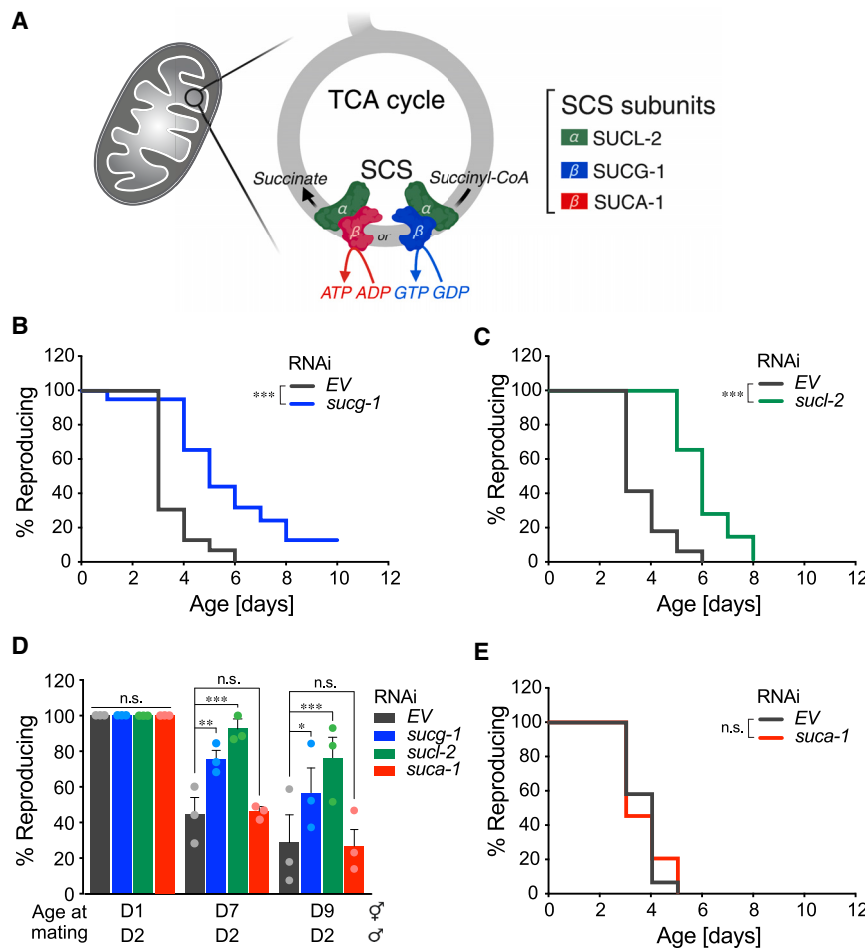
Figure 1. GTP-specific succinyl-CoA synthetase (SCS) regulates reproductive aging

(A) A diagram of SCS enzymatic function and its ATP or GTP specificity.

(B) Wild-type (WT) worms subjected to *sucg-1* RNA interference (RNAi) have a significantly longer reproductive lifespan (RLS) than those subjected to the empty vector (EV) control.

(C) WT worms subjected to *sucl-2* RNAi have a longer RLS than those subjected to the EV control.

(D) Day-7 and -9 WT hermaphrodites subjected to *sucg-1* or *sucl-2* but not *suca-1* RNAi show higher rates of reproduction than those subjected to the EV control, when mated with 2-day-old males.

(E) WT worms subjected to *suca-1* RNAi show no significant differences in RLS, compared with those subjected to the EV control.

(B), (C), and (E) n.s. $p > 0.05$ and ***$p < 0.001$ by log rank test; n = 3 biological independent replicates, ~20 worms per replicate, see Table S1 for full RLS data. (D) Error bars represent mean ± SEM, n = 3 biologically independent samples, n.s. $p > 0.05$, *$p < 0.05$, **$p < 0.01$, and ***$p < 0.001$ by Fisher's exact test adjusted with the Holm-Bonferroni method for multiple comparisons, ~20 worms per replicate.

drial fission selectively in the germ line prevents age-associated perinuclear accumulation of oocyte mitochondria and promotes reproductive longevity in *C. elegans*. Furthermore, we found that the regulation of reproductive aging by GTP-specific SCS and mitochondrial fission-fusion factors responds to the level of vitamin B12 (VB12) in bacteria. These findings suggest a previously unknown function of mitochondrial GTP (mtGTP) metabolism in the germ line and its significance in the regulation of mitochondrial homeostasis and oocyte quality during aging.

RESULTS

GTP-specific SCS regulates reproductive aging

In *C. elegans*, succinyl-CoA ligase *(sucl-2)* and succinyl-CoA ligase, GTP-specific *(sucg-1)* encode the alpha and the GTP-specific beta subunit of SCS, respectively (Figure 1A). We found that inactivating either *sucl-2* or *sucg-1* by RNAi not only extends reproductive lifespan (RLS) but also improves fertility in aged hermaphrodites (late fertility) (Figures 1B–1D; Table S1). As the age of hermaphrodites increased from 1 to 7 and 9 days old, the percentage of individuals capable of reproducing decreased from 100% to less than 50% and 30%, respectively, when they were mated with 2-day-old young males (Figure 1D). With *sucg-1* or *sucl-2* RNAi knockdown (KD), the percentage of aged hermaphrodites capable of reproducing increased to more than 70% or 90% on day 7 and more than 50% or 70% on day 9, respectively (Figure 1D).

Next, we examined *suca-1* that encodes the ATP-specific beta subunit and found that its RNAi KD does not extend RLS or improve late fertility (Figures 1D and 1E; Table S1). These results

of mitochondrial fission-fusion factors in oocyte quality control during development.

On the other hand, in *Caenorhabditis elegans*, mitochondrial fission-fusion factors have been linked with the regulation of somatic aging. Selectively overexpressing the *C. elegans* DRP1 homolog *drp-1* in the intestine prolongs lifespan,[14] and whole-body KO of *drp-1* together with fuzzy onions related *(fzo)-1*, the *C. elegans* MFN homolog, leads to lifespan extension in *C. elegans*.[15] Besides being a well-established model organism for studying somatic aging, *C. elegans* shares similarities with humans regarding reproductive aging.[16] Both genetic factors and environmental cues including bacterial inputs are known to regulate reproductive aging in *C. elegans*.[17] Through a full-genome RNA interference (RNAi) screen, we identified two subunits of mitochondrial succinyl-coenzyme A (CoA) synthetase (SCS) as regulators of reproductive aging.[18] SCS is a key mitochondrial enzyme in the tricarboxylic acid (TCA) cycle converting succinyl-CoA to succinate with a production of guanosine triphosphate (GTP) or ATP.[19] A functional SCS enzyme comprises one alpha subunit and one beta subunit. Two interchangeable beta subunits of SCS determine the GTP/ATP specificity by forming a complex with the constant alpha subunit.[20,21]

In this study, we discovered that GTP-specific SCS in the germ line regulates reproductive aging through tuning mitochondrial positioning in the oocyte and that increasing mitochon-
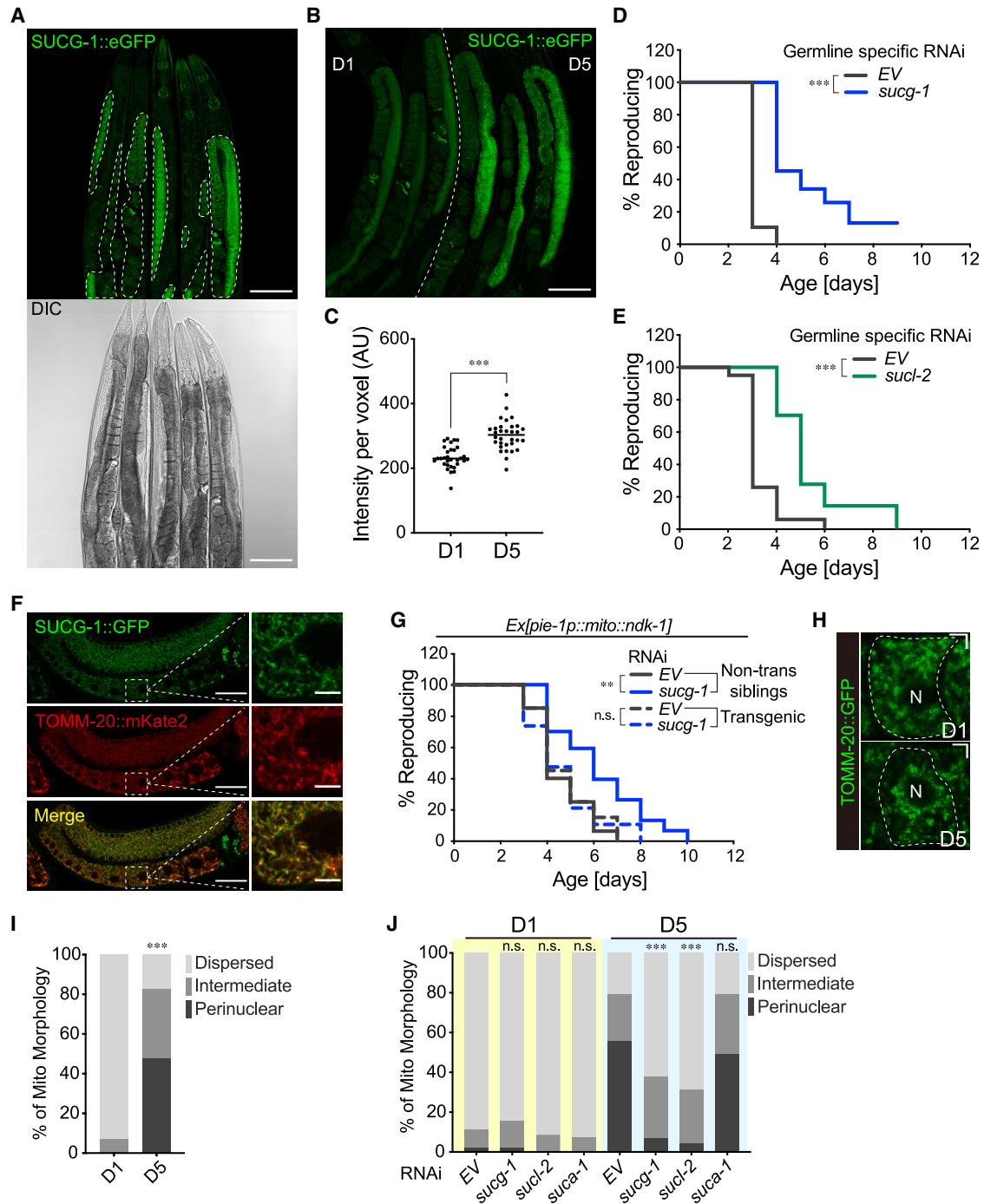
Figure 2. GTP-specific SCS functions in the germ line to regulate oocyte mitochondria during reproductive aging

(A) Confocal imaging of the SUCG-1::eGFP knockin line, in which the endogenous *sucg-1* is tagged with *egfp*, shows its predominant expression in the germ line but weak expression in the intestine, pharynx, muscle, hypodermis, and neurons. Scale bars, 100 μm; dashed white line: germ line.

(B) The SUCG-1::eGFP level in the germ line is increased at day 5 compared with day 1. Scale bars, 100 μm.

(C) Quantification of SUCG-1::eGFP level in the germ line at day 1 and day 5. a.u., arbitrary unit.

(D) Germline-specific RNAi inactivation of *sucg-1* extends RLS.

(E) Germline-specific RNAi inactivation of *sucl-2* extends RLS.

(F) SUCG-1::eGFP co-localizes with mitochondrial TOMM-20::mKate2 in the germ line. Scale bars: 30 μm for the images with lower magnification and 5 μm for the images with higher magnification.

(G) Overexpression of mitochondria-targeted *ndk-1*(*mito::ndk-1*) in the germ line suppresses the RLS extension caused by *sucg-1* RNAi knockdown.

(legend continued on next page)

suggest that the SCS complex formed by the alpha subunit SUCL-2 and the beta subunit SUCG-1 is specifically involved in regulating RLS and late fertility. Given that SUCG-1 is responsible for converting guanosine diphosphate (GDP) to GTP in mitochondria, these results indicate a possible role of mtGTP metabolism in modulating reproductive aging.

Germline GTP-specific SCS regulates mitochondria and reproductive aging

To understand how the GTP-specific SCS regulates reproductive aging, we first examined the expression pattern of *sucg-1* using a CRISPR knockin (KI) line in which endogenous SUCG-1 is tagged with enhanced green fluorescent protein (eGFP) at the C terminus. SUCG-1::eGFP expresses predominantly in the germ line, with weaker signals in the pharynx, intestine, hypodermis, and muscle (Figure 2A). Using CRISPR KI, endogenous SUCA-1 was also tagged with eGFP at the C terminus, which showed the predominant expression in the pharynx, neuron, intestine, hypodermis, and muscle but a very weak yet detectable signal in the germ line (Figure S1A). Moreover, we found that the GFP intensity in the germ line of the SUCG-1::eGFP worms is increased at day 5 compared with day 1 (Figures 2B and 2C), suggesting an elevation of germline SUCG-1 levels with age. These findings suggest that mitochondrial SUCG-1 may function in the germ line to regulate reproductive aging cell autonomously.

To further confirm this cell-autonomous regulation, we utilized a tissue-specific RNAi strain in which the expression of the RNAi-induced silencing complex component RNAi defective (RDE-1) is restored specifically in the germ line of the *rde-1* null mutant.[22] We knocked down either *sucg-1* or *sucl-2* by RNAi selectively in the germ line and found that germline-specific KD of *sucg-1* extends RLS, compared with control worms treated with the empty vector (EV) (Figure 2D; Table S1). Germline-specific KD of *sucl-2* led to similar RLS-extending effects (Figure 2E; Table S1). These results suggest that *sucg-1* and *sucl-2* act in the germ line to regulate reproductive longevity. We also measured the progeny number in those worms and observed 7% or 11% reduction associated with the *sucg-1* or *sucl-2* germline-specific RNAi KD, respectively (Figures S1B and S1C). The decrease in the progeny number has been previously observed in other interventions leading to RLS extension, such as the loss-of-function mutant of *daf-2*, eating, abnormal (*eat*)-2, and *sma-2*.[23–26] In addition, the *daf-2* and the *eat-2* mutants not only prolong RLS but also extend lifespan.[27,28] We found that the whole-body RNAi KD of either *sucg-1* or *sucl-2* leads to a mild lifespan extension (~15%), but *suca-1* KD does not affect lifespan (Figure S1D; Table S2). Upon germline-specific RNAi KD, the result was similar except that *sucg-1* showed no lifespan extension in one out of three trials, and *suca-1* showed a slightly shortened lifespan in one out of three trials (Figure S1E; Table S2).

Both GTP- and ATP-specific SCS catalyze succinate production from succinyl-CoA, and their losses lead to increased succinyl-CoA and decreased succinate levels. However, RNAi KD of *suca-1* and *sucg-1* exerted distinctive effects on RLS, suggesting that the change in either succinate or succinyl-CoA level is unlikely linked with the observed reproductive longevity phenotype. In support of this idea, we found that dietary supplementation of sodium succinate or succinic acid does not alter RLS (Figure S1F; Table S1). Additionally, germline-specific KD of *ogdh-1*, which encodes a subunit of α-ketoglutarate dehydrogenase (upstream of SCS), led to sterility and production of dead eggs that failed to hatch despite having an intact germ line. Meanwhile, germline-specific KD of *mev-1* or *sdhb-1* encoding subunits of succinate dehydrogenase (downstream of SCS) resulted in a very short reproductive time window (Figure S1G; Table S1). Together, these results suggest that GTP-specific SCS reduction in the germ line promotes reproductive longevity, which is unlikely due to altered succinate or succinyl-CoA levels.

Next, we crossed the *sucg-1::egfp* line with the transgenic strain that expresses mKate2-tagged translocase of outer mitochondrial membrane (TOMM)-20 on the outer mitochondrial membrane (OMM) in the germ line.[29] The co-localization between SUCG-1::eGFP and TOMM-20::mKate2 (Figure 2F) confirms the mitochondrial localization of SUCG-1. To test whether SUCG-1 regulates reproductive longevity through affecting mtGTP levels in the germ line, we made a transgenic strain expressing mitochondrial matrix-targeting sequence-tagged *ndk-1* specifically in the germ line. *ndk-1* encodes the nucleoside diphosphate kinase that catalyzes GTP synthesis from ATP, and thus its overexpression would increase GTP levels.[30] We found that *ndk-1* overexpression in germline mitochondria is sufficient to suppress the RLS extension caused by *sucg-1* KD (Figure 2G; Table S1), suggesting that GTP-specific SCS regulates reproductive aging through modulating mtGTP levels in the germ line.

To test whether the loss of SCS affects germline mitochondrial homeostasis, we utilized the transgenic strain expressing GFP-tagged TOMM-20 in the germ line[29] and imaged mitochondrial morphology at day 1 and day 5. We found that mitochondrial fragmentation and tubulation morphology exhibit high variations between individuals of the same genotype, which prevented us from drawing an explicit conclusion. On the other hand, we observed that the mitochondrial network of oocytes increases perinuclear distribution in day-5 aged worms, while being largely dispersed in day-1 young worms (Figure 2H). We wrote an imaging analysis script to quantify mitochondrial signals in five rings of oocyte cells and classified mitochondrial distribution into three categories—dispersed, intermediate, and perinuclear (Figure S2A). We found that mitochondrial GFP signals are evenly distributed throughout the five rings in the oocyte of day-1

(H) Representative images show that oocyte mitochondria are largely dispersed at day 1 while experiencing increasing perinuclear distribution at day 5. Scale bars, 5 μm; dashed white line: oocyte outline; N, nucleus.

(I) Perinuclear clustering of oocyte mitochondria is increased from day 1 to day 5.

(J) The increase in perinuclear distribution of oocyte mitochondria at day 5 is suppressed by *sucg-1* or *sucl-2* but not by *suca-1* RNAi knockdown.

(C) ***p < 0.001 by Student's t test; n = 31 (day 1) and n = 32 (day 5). (D), (E), and (G) **p < 0.01 and ***p < 0.001 by log rank test; n = 4 (in D) or 3 (in E and G) biological independent replicates, ~20 worms per replicate, see Table S1 for full RLS data. (I) n = 43 (day 1), n = 40 (day 5); ***p < 0.001 by chi-squared test. (J) n = 45 (EV, day 1), n = 45 (*sucg-1*, day 1), n = 45 (*sucl-2*, day 1), n = 45 (*suca-1*, day 1), n = 42 (EV, day 5), n = 45 (*sucg-1*, day 5), n = 44 (*sucl-2*, day 5), and n = 48 (*suca-1*, day 5); RNAi vs. EV, n.s. p > 0.05 and ***p < 0.001 by chi-squared test adjusted with the Holm-Bonferroni method for multiple comparisons.

worms (Figure S2B), while in the oocyte of day-5 worms, the percentage of the mitochondrial GFP signal derived from the perinuclear ring 1 is increased (Figures S2B and S2C). Further categorization analysis identified that the perinuclear distribution of oocyte mitochondria is increased in day-5 worms (Figure 2I). To test whether this change in mitochondrial distribution is associated with a decrease in mitochondrial content, we first measured mitochondrial DNA (mtDNA) levels in the dissected germ line using quantitative PCR (qPCR). The result showed that the mtDNA level is 60% higher in the germ line of day-5 worms than in that of day-1 worms (Figure S2D). Next, we measured mtDNA copy numbers in isolated oocytes using droplet digital PCR (ddPCR) and found no difference between oocytes of day-1 and day-5 worms (Figure S2E). These results indicate that the age-associated perinuclear accumulation of oocyte mitochondria is unlikely due to a decline in mitochondrial numbers.

Interestingly, we found that RNAi KD of *sucg-1* or *sucl-2* suppresses the age-associated increase in mitochondrial clustering around the nucleus, while RNAi KD of *suca-1* shows no such effect (Figures 2J and S3A), which are consistent with their effects on RLS and late fertility (Figures 1B–1E). Furthermore, *sucg-1*, *sucl-2*, or *suca-1* germline-specific RNAi KD did not affect the germline mtDNA level at day 1 (Figure S2F). At day 5, worms with *sucg-1*, *sucl-2*, or *suca-1* germline-specific RNAi KD exhibited similar germline mtDNA levels, which were ∼30% higher than those of control worms (Figure S2F). Thus, the loss of either SCS isoform increases mitochondrial content in the germ line with aging, which is not specific to *sucg-1* KD and thus unlikely related to its effect on oocyte mitochondrial positioning. Together, we found that GTP-specific SCS works specifically in the germ line to regulate oocyte mitochondrial distribution during reproductive aging.

Mitochondrial fission drives reproductive longevity

Mitochondrial distribution is modulated by the dynamin family of GTPases.[9] To determine whether these GTPases regulate reproductive aging, we examined EAT-3, FZO-1, and DRP-1, which are *C. elegans* homologs of human OPA1, MFN1/2, and DRP1, respectively.[31] EAT-3 drives inner mitochondrial membrane (IMM) fusion while FZO-1 is responsible for the fusion of the OMM (Figure 3A).[32,33] We found that germline-specific RNAi KD of *eat-3* increases RLS and late fertility (Figures 3B and 3C; Table S1). Meanwhile, *fzo-1* KD selectively in the germ line did not affect late fertility (Figure 3C), and it only showed slight RLS extension (11.5%) in one out of three trials (Figure 3D; Table S1). Thus, in the germ line, EAT-3-mediated IMM fusion is involved in regulating reproductive aging. The *eat-3* mutant was originally discovered showing abnormal pharyngeal pumping and food intake, like the *eat-2* mutant.[34] The *eat-2* mutant is known to slow down reproductive aging as a result of caloric restriction.[27,34] To test whether the effect of *eat-3* on reproductive aging is also due to a reduction in food intake, we measured the pharyngeal pumping rate and the body size in worms with germline-specific *eat-3* RNAi KD and found no alterations (Figures S4A–S4C), suggesting that the RLS extension does not result from caloric restriction.

In contrast to EAT-3 and FZO-1, DRP-1 drives mitochondrial fission (Figure 3A).[35,36] When we knocked down *drp-1* by RNAi

selectively in the germ line, we found that RLS either remains unchanged (in two replicates) or is slightly decreased (in one replicate), and late fertility is not altered in these worms (Figures 3C and 3E; Table S1). Conversely, when we overexpressed *drp-1* selectively in the germ line, transgenic worms showed an extremely long RLS compared with controls (Figure 3F; Table S1). Together, these results show that increasing mitochondrial fission factors and decreasing inner mitochondrial fusion factors in the germ line are both sufficient to promote reproductive longevity.

Next, we examined whether these mitochondrial fission-fusion factors regulate oocyte mitochondrial distribution. We found that in the *drp-1* germline-specific overexpression transgenic strain, the age-associated perinuclear accumulation of oocyte mitochondria is greatly suppressed in day-5 aged worms (Figures 3G and S3B). RNAi KD of *eat-3* also decreased the perinuclear accumulation of oocyte mitochondria at day 5 (Figures 3H and S3A). However, RNAi KD of *fzo-1* did not affect oocyte mitochondrial distribution in either day-1 or day-5 worms (Figures 3H and S3A). Upon *drp-1* RNAi KD, we observed an increase in the perinuclear distribution of oocyte mitochondria in day-1 worms, which however did not reach statistical significance (Figures 3H and S3A). In day-5 worms, *drp-1* RNAi KD caused disruption in oocyte organization, and mitochondrial morphology became largely unscorable (Figures 3H and S3C). In the few oocytes that still had recognizable cell boundaries, we observed one-sided perinuclear aggregation of mitochondria (Figure S3A). These results suggest that mitochondrial fission-fusion factors modulate mitochondrial distribution in oocytes, which correlates with their regulatory effects on reproductive aging.

GTP-specific SCS regulates reproductive aging through tuning mitochondrial distribution

We then asked whether the change in mitochondrial distribution is responsible for the reproductive longevity-promoting effect conferred by *sucg-1* KD. To answer this question, we utilized an auxin-inducible degron (AID) system to deplete the DRP-1 protein specifically in the germ line upon the auxin treatment (Figure 4A). We first generated a CRISPR KI line *(gfp::degron::drp-1)* in which endogenous DRP-1 is tagged with GFP and degron at the N terminus.[37] This line was next crossed with the single-copy integrated transgenic strain where the auxin-inducible F-box protein transport inhibitor response 1 (TIR1) is selectively expressed in the germ line *(sun-1p::TIR1::mRuby)*.[38] Using this system, auxin administration led to TIR1-mediated degradation of the degron-tagged DRP-1 protein in the germ line but not in other tissues (Figure 4B). We found that the auxin-induced DRP-1 depletion in the germ line causes no significant change in RLS (Figure 4C; Table S1), recapitulating the finding from germline-specific RNAi KD of *drp-1* (Figure 3E). More importantly, although the germline-specific DRP-1 depletion did not affect RLS on its own, it fully suppressed the RLS extension caused by *sucg-1* RNAi KD (Figure 4D; Table S1).

Furthermore, the *drp-1* loss-of-function mutant increased perinuclear clustering of oocyte mitochondria at day 1, and *sucg-1* RNAi KD failed to suppress this increase (Figures 4E and S3D), which suggests the requirement of DRP-1 for the loss of SUCG-1 to drive oocyte mitochondrial dispersion. Therefore, mtGTP metabolism can regulate reproductive longevity by
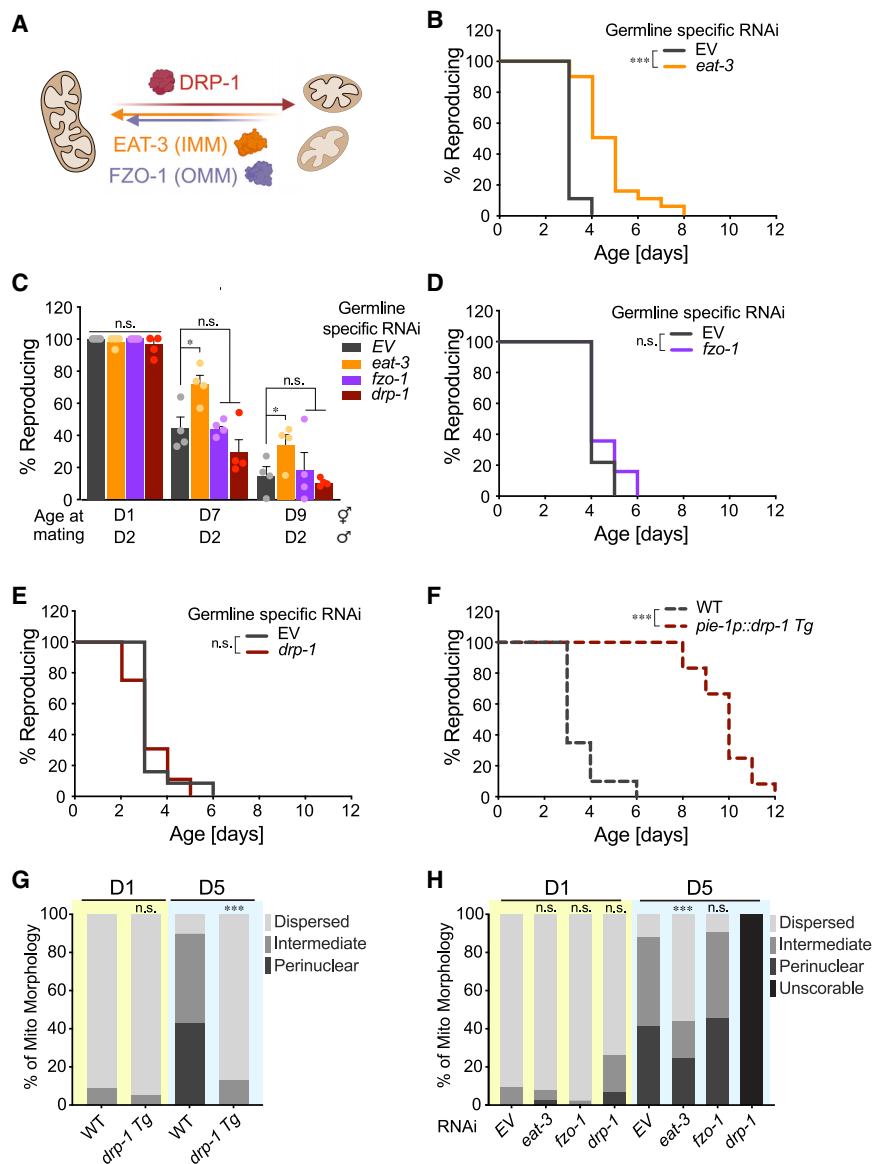
Figure 3. Mitochondrial fission-fusion factors regulate reproductive longevity

(A) A diagram showing regulation of mitochondrial fission-fusion by GTPase DRP-1, FZO-1, and EAT-3. IMM, inner mitochondrial membrane; OMM, outer mitochondrial membrane.

(B) Germline-specific RNAi inactivation of *eat-3* extends RLS.

(C) Day-7 and -9 aged hermaphrodites subjected to germline-specific *eat-3* RNAi have a higher rate of reproduction than those subjected to the EV control, when mated with 2-day-old young males, while germline-specific RNAi inactivation of *fzo-1* or *drp-1* RNAi does not affect the rate of reproduction at all ages.

(D) Germline-specific RNAi inactivation of *fzo-1* does not affect RLS.

(E) Germline-specific RNAi inactivation of *drp-1* does not affect RLS.

(F) Germline-specific overexpression of *drp-1* prolongs RLS.

(G) The perinuclear clustering of oocyte mitochondria at day 5 is decreased in the transgenic strain with germline-specific *drp-1* over-expression.

(H) The increase in the perinuclear distribution of oocyte mitochondria at day 5 is decreased upon *eat-3* but not *fzo-1* RNAi knockdown. The distribution of oocyte mitochondria is not scorable in day-5 aged worms subjected to *drp-1* RNAi knockdown due to distorted germ line.

(B) and (D)–(F) n.s. $p > 0.05$ and ***$p < 0.001$ by log rank test; n = 3 biological independent replicates, ~20 worms per replicate, see Table S1 for full RLS data. (C) Error bars represent mean ± SEM, n = 4 biologically independent samples, n.s. $p > 0.05$ and *$p < 0.05$ by Fisher's exact test adjusted with the Holm-Bonferroni method for multiple comparisons, ~15 worms per replicate. (G) n = 46 (WT, day 1), n = 42 (*drp-1 OE*, day 1), n = 40 (WT, day 5), and n = 46 (*drp-1 OE*, day 5); WT vs. *drp-1 OE*, n.s. $p > 0.05$ and ***$p < 0.001$ by chi-squared test. (H) n = 43 (EV, day 1), n = 38 (*eat-3*, day 1), n = 40 (*fzo-1*, day 1), n = 46 (*drp-1*, day 1), n = 41 (EV, day 5), n = 41 (*eat-3*, day 5), and n = 42 (*fzo-1*, day 5); RNAi vs. EV, n.s. $p > 0.05$ and ***$p < 0.001$ by chi-squared test adjusted with the Holm-Bonferroni method for multiple comparisons.

affecting mitochondrial positioning in the germ line through a DRP-1-mediated mechanism.

GTP-specific SCS regulates reproductive aging in response to bacterial inputs

To confirm the difference between *sucg-1* and *suca-1* in regulating reproductive aging, we generated their CRISPR KO lines (Figure S5A). *suca-1* KO worms were phenotypically wild type (WT), and similarly to the RNAi KD worms, they did not show an RLS change (Figures S5B and S5C; Table S1). On the other hand, while *sucg-1* homozygous KO worms appeared WT in the parental generation, their progeny exhibited delayed development because of maternal *sucg-1* deficiency. To avoid this maternal effect, we generated a heterozygous parental line by crossing the *sucg-1* KO line with the *sucg-1::egfp* KI line (GFP) (Figure 5A). This way, we could examine the reproductive pheno-

type of the progeny that carries the following genotypes, KO/KO, KO/GFP, and GFP/GFP, on the *sucg-1* locus (Figure 5A). We found that the *sucg-1* homozygous KO/KO worms have extended RLS, compared with either KO/GFP heterozygous or GFP/GFP homozygous worms (Figures 5B and S5D; Table S1). These results confirm the specificity of GTP-specific SCS in regulating reproductive aging.

When examining these KO mutant worms, we also had an interesting observation that on Escherichia coli OP50 (OP50 *E. coli*), neither the *sucg-1* nor the *suca-1* homozygous KO caused an RLS extension (Figures 5C and S5E–S5G; Table S3). Previous findings in our lab identified that *C. elegans* shows distinct reproductive strategies when exposed to different bacteria. WT worms that host OP50 *E. coli* have a longer RLS and improved late fertility than those on HB101 *E. coli*, while WT worms on HT115 *E. coli* had similar RLS and late fertility to those
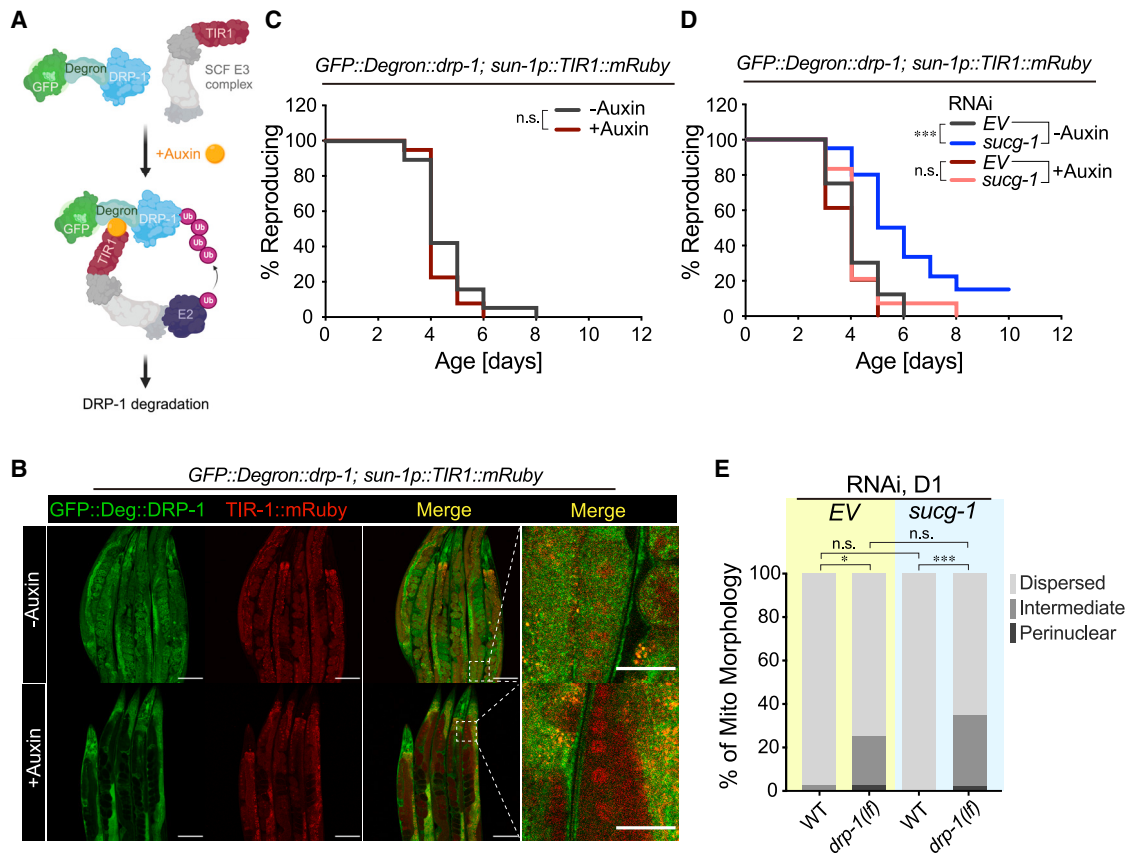
Figure 4. GTP-specific SCS regulates reproductive aging through mitochondrial fission factor

(A) A diagram demonstrating auxin-induced degradation of endogenous DRP-1 tagged with GFP and degron.

(B) Confocal imaging of GFP shows that the endogenous DRP-1 protein is specifically depleted in the germ line upon the auxin treatment. Scale bars: 100 μm for the images with lower magnification and 30 μm for the images with higher magnification.

(C) Auxin-induced germline-specific depletion of DRP-1 does not affect RLS.

(D) Auxin-induced germline-specific depletion of DRP-1 abrogates the RLS extension caused by *sucg-1* RNAi.

(E) The *drp-1* loss-of-function mutant increases the perinuclear clustering of oocyte mitochondria at day 1, which is not suppressed by *sucg-1* RNAi knockdown. (C) and (D) n.s. $p > 0.05$ and ***$p < 0.001$ by log rank test; n = 3 biological independent replicates, ∼20 worms per replicate, see Table S1 for full RLS data. (E) n = 38 (WT, EV RNAi, day 1), n = 41 (*drp-1(tm1108)*, EV RNAi, day 1), n = 41 (WT, *sucg-1* RNAi, day 1), and n = 46 (*drp-1(tm1108)*, *sucg-1* RNAi, day 1); RNAi vs. EV and WT vs. *drp-1* mutant, n.s. $p > 0.05$, *$p < 0.05$, and ***$p < 0.001$ by chi-squared test adjusted with the Holm-Bonferroni method for multiple comparisons.

on HB101[17] (Figures S6A and S6B; Table S1). For the germline-specific RNAi KD of *sucg-1*, *sucl-2*, or *suca-1*, the experiments were conducted in the background of HT115 *E. coli* (Figures 2D, 2E, and S6C; Table S1). When we examined their effects in the background of OP50 *E. coli*, we found that none of them enhances the RLS extension caused by OP50 (Figures S6D–S6F; Table S3). These results suggest that different *E. coli* may affect mtGTP to exert different effects on worm reproductive aging.

To examine whether bacterial inputs affect mtGTP levels in the germ line, we utilized the transgenic strain where germline mitochondria were tagged with GFP and triple Hemagglutinin (HA) and purified mitochondria using anti-HA magnetic beads via immunoprecipitation. We then measured germline mtGTP using liquid chromatograph coupled with mass spectrometry. We found that in the germ line of day-5 worms on HT115 *E. coli*, the mtGTP level is increased by nearly 10-fold, compared with day-1 worms, but the mtGTP induction level is only around 3-fold in the germ line of worms on OP50 *E. coli* (Figure 5D).

Moreover, day-5 worms on HT115 *E. coli* had a higher germline mtGTP level compared with that of worms on OP50 *E. coli*, while no difference in the germline mtGTP level was observed in day-1 worms (Figure 5D). On the other hand, the germline mitochondrial ATP (mtATP) levels were comparable between worms at different ages or on different bacteria (Figure 5E). These results suggest that reproductive longevity conferred by OP50 *E. coli* may be linked to an attenuation in the age-related increase in GTP production.

Bacteria modulate mitochondrial distribution during reproductive aging

Next, we examined whether OP50 *E. coli* causes changes in oocyte mitochondrial distribution using the TOMM-20::GFP strain. When compared with worms on HT115 *E. coli*, worms on OP50 *E. coli* attenuated the age-associated increase in the perinuclear clustering of oocyte mitochondria (Figures 6A and S3E). Moreover, germline-specific depletion of the DRP-1
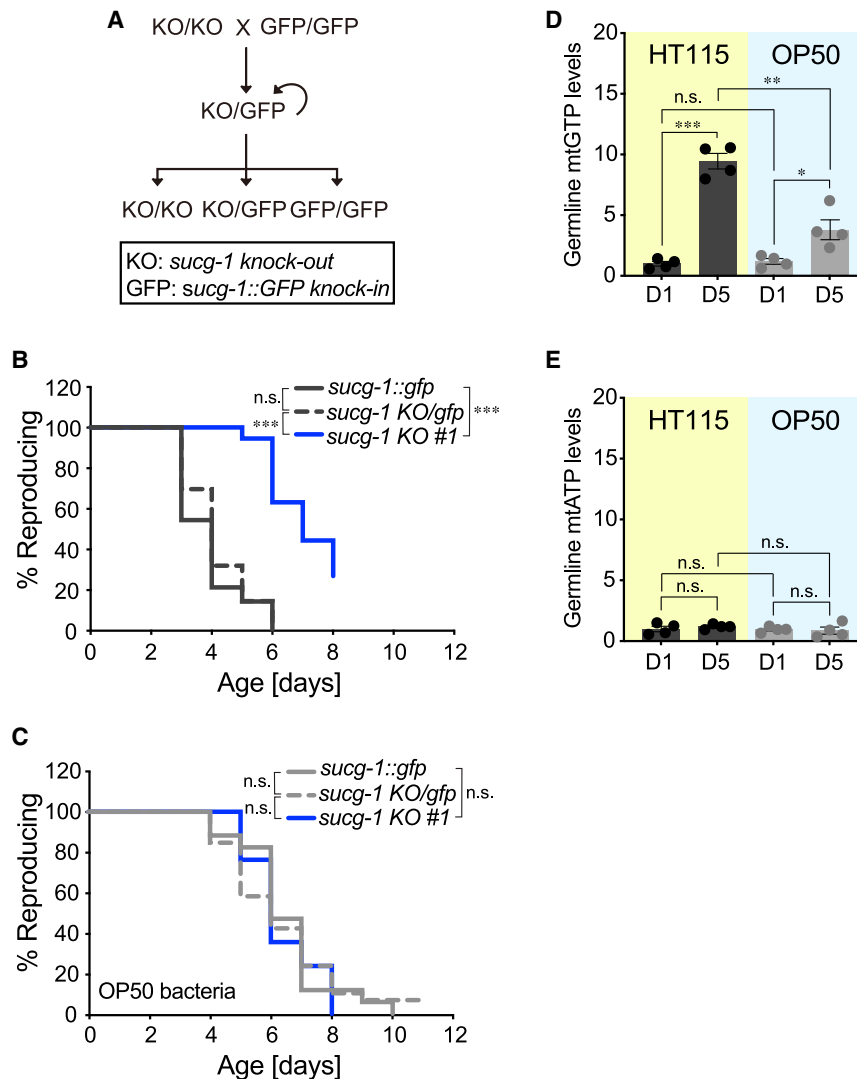
Figure 5. Bacterial inputs regulate germline mitochondrial GTP and reproductive aging

(A) A diagram showing the strategy to obtain *sucg-1* homozygous knockout (KO) mutants from heterozygous mutants with *sucg-1* KO at one locus and *sucg-1::egfp* (GFP) at the other locus.

(B) *sucg-1* KO/KO mutants show a significant increase in RLS, compared with *sucg-1* GFP/GFP and *sucg-1* KO/GFP worms.

(C) With OP50 bacteria, *sucg-1* KO/KO mutants show no significant differences in RLS, compared with *sucg-1* GFP/GFP or *sucg-1* KO/GFP worms.

(D) Germline mitochondrial GTP (mtGTP) level is increased by 9.4-fold in day-5 aged worms compared with day-1 young worms on HT115 bacteria. With OP50 bacteria, the germline mtGTP level increase from day 1 to day 5 is 3-fold. The germline mtGTP level is higher in worms on HT115 bacteria than those on OP50 bacteria at day 5 but not at day 1.

(E) Germline mitochondrial ATP (mtATP level) is not significantly different in worms of different ages and on different bacteria.

(B) and (C) n.s. $p > 0.05$ and ***$p < 0.001$ by log rank test; n = 3 biological independent replicates, ~80 worms per replicate split into 3 genotypes, see Table S1 (B) and Table S3 (C) for full RLS data.

(D) and (E): error bars represent mean ± SEM, n = 4 biologically independent samples, n.s. $p > 0.05$, *$p < 0.05$, **$p < 0.01$, and ***$p < 0.001$ by Student's t test adjusted with the Holm-Bonferroni method for multiple comparisons.

protein or the germline-specific RNAi KD of *drp-1* fully suppressed the RLS extension in worms on OP50 *E. coli* (Figures 6B and S6G; Table S3). In addition, with the AID system, we could apply the auxin treatment selectively during adulthood, leading to DRP-1 loss after the germ line completes development and switches from spermatogenesis to oogenesis. We found that this adult-only depletion of DRP-1 in the germ line suppresses the RLS extension in worms on OP50 *E. coli* (Figure 6C; Table S3), supporting the significance of oocyte mitochondrial distribution in regulating reproductive aging. Furthermore, germline-specific overexpression of *drp-1* increases RLS in worms on either HT115 (Figure 3F; Table S1) or OP50 *E. coli* (Figure 6D; Table S3), whereas germline-specific RNAi KD of *eat-3* failed to further enhance the RLS extension in worms on OP50 *E. coli* (Figure 6E; Table S3). Like in worms on HT115 *E. coli*, germline-specific RNAi KD of *fzo-1* did not alter RLS in worms on OP50 *E. coli* (Figure S6H; Table S3).

Furthermore, we found that *drp-1* RNAi KD largely disturbs oocyte organization and mitochondrial distribution in day-5 worms on OP50 *E. coli* (Figures 6F and S3G), and in the small percentage of oocytes with recognizable cell boundaries, one-sided perinuclear aggregation of mitochondria was observed (Figure S3F). On the other hand, RNAi KD of either *eat-3* or *fzo-1* had no effects on oocyte mitochondrial distribution in worms on OP50 *E. coli* (Figures 6F and S3F). RNAi KD of *sucg-1*, *sucl-2*, or *suca-1* could not alter oocyte mitochondrial distribution in worms on OP50 *E. coli* either (Figures S3F and S6I). Together, these results suggest that like GTP-specific SCS, OP50 bacterial inputs modulate mitochondrial distribution and reproductive longevity via mitochondrial fission-fusion factors.

VB12 deficiency in OP50 *E. coli* contributes to reproductive longevity

Our previous study identified that the trace amount of HB101 mixing in OP50 *E. coli* is sufficient to shorten RLS, suggesting the involvement of bioactive metabolites in regulating reproductive aging. Interestingly, it has been shown that OP50 *E. coli* is low in VB12, and the VB12 level affects mitochondrial dynamics in worm muscle.[39–42] We monitored VB12 levels using the transgenic strain expressing the *acdh-1p::gfp* reporter[39,40] and found that GFP intensity is ~2.5-fold higher in worms on OP50 than those on HT115 *E. coli* (Figures 7A and 7B). To test whether VB12 deficiency could contribute to reproductive longevity, we supplied two different forms of VB12, methylcobalamin (meCbl) and adenosylcobalamin (adoCbl), to worms on OP50 and HT115
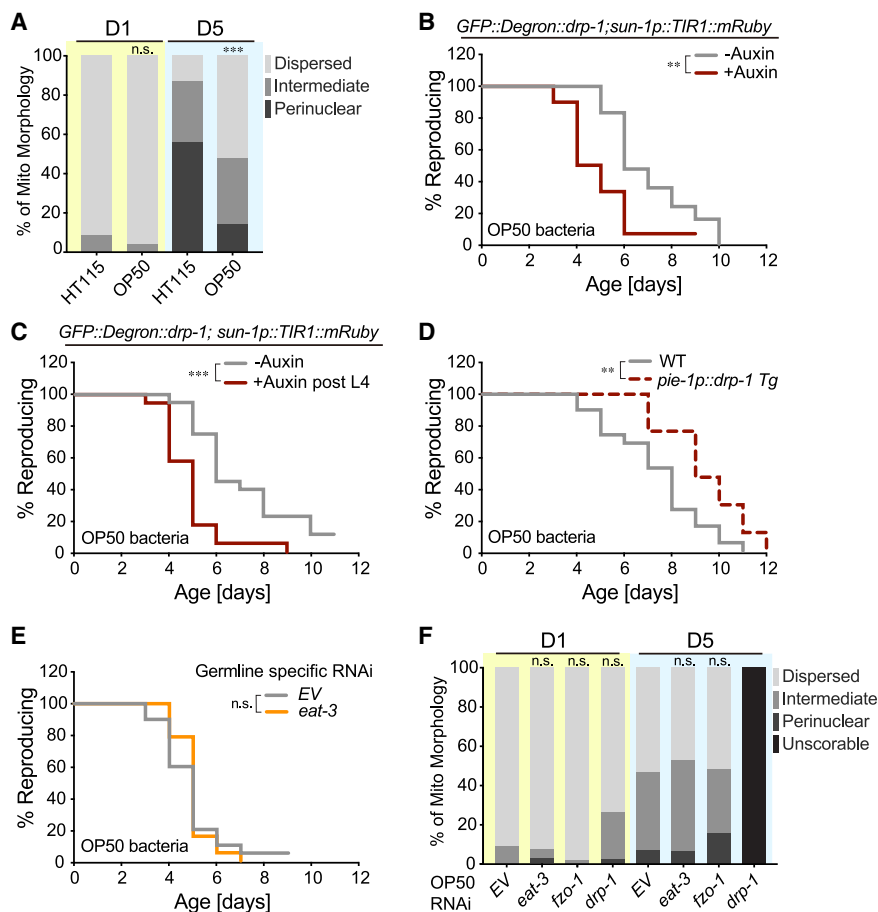
Figure 6. Mitochondrial fission-fusion factors mediate bacterial effects on reproductive longevity

(A) The perinuclear clustering of oocyte mitochondria is decreased in day-5 worms on OP50, compared with those on HT115 bacteria.

(B) Auxin-induced germline-specific depletion of DRP-1 reduces RLS in worms on OP50 bacteria.

(C) Adult-only germline-specific depletion of DRP-1 reduces RLS in worms on OP50 bacteria.

(D) Germline-specific overexpression of *drp-1* prolongs RLS in worms on OP50 bacteria.

(E) Germline-specific RNAi inactivation of *eat-3* fails to extend RLS in worms on OP50 bacteria.

(F) With OP50 bacteria, the distribution of oocyte mitochondria is not significantly different between EV control worms and those subjected to *eat-3* or *fzo-1* RNAi knockdown at day 5. With *drp-1* RNAi knockdown, oocyte mitochondrial distribution becomes unscorable due to distorted germ line.

(A) n = 48 (HT115, day 1), n = 53 (OP50, day 1), n = 47 (HT115, day 5), and n = 48 (OP50, day 5); HT115 vs. OP50, n.s. $p > 0.05$ and ***$p < 0.001$ by chi-squared test. (B)–(E) n.s. $p > 0.05$, **$p < 0.01$, and ***$p < 0.001$ by log rank test; n = 3 (in B–D) or 4 (in E) biological independent replicates, ~20 worms per replicate, see Table S3 for full RLS data. (F) n = 44 (EV, day 1), n = 43 (*eat-3*, day 1), n = 41 (*fzo-1*, day 1), n = 42 (*drp-1*, day 1), n = 43 (EV, day 5), n = 43 (*eat-3*, day 5), and n = 43 (*fzo-1*, day 5); OP50 condition; RNAi vs. EV, n.s. $p > 0.05$ by chi-squared test adjusted with the Holm-Bonferroni method for multiple comparisons.

E. coli. We discovered that supplementation of either meCbl or adoCbl reduces the RLS extension in worms on OP50 *E. coli* but does not affect RLS in worms on HT115 *E. coli* (Figures 7C and S7A–S7C; Tables S1 and S3). In addition, meCbl supplementation increased the perinuclear accumulation of oocyte mitochondria in day-5 worms on OP50 *E. coli* (Figures 7D and S3H) to a level similar to that of worms on VB12-sufficient HT115 *E. coli*. These results suggest that bacteria-derived VB12 plays a crucial role in regulating oocyte mitochondrial distribution and reproductive aging.

We further examined whether VB12 signals through GTP-specific SCS to modulate reproductive aging. We found that although the *sucg-1* heterozygous mutant (KO/GFP) and *gfp* homozygous (GFP/GFP) worms on OP50 *E. coli* experience a decrease in RLS when supplied with meCbl, this was not observed in the *sucg-1* homozygous (KO/KO) mutant worms (Figures 7E, S7D, and S7E; Table S3). This result suggests that SUCG-1 is required for VB12 to regulate reproductive aging. Two enzymes utilize VB12 as the co-factor for their functions, namely methylmalonylCoA mutase (MMCM)-1, a mitochondrial enzyme that converts methymalonyl-CoA to succinyl-CoA, and 5-methyltetrahydrofolate-homocysteine methyltransferase (METR)-1, the methionine synthase (MTR) that converts homocysteine to methionine. We discovered that *mmcm-1* RNAi KD does not affect RLS in worms on either OP50 or HT115 *E. coli* (Figures S7F and S7G; Tables S1 and

S3). These results further support that succinyl-CoA is not involved in the regulation of reproductive aging. On the other hand, *metr-1* RNAi KD increased RLS in worms on HT115 but not OP50 *E. coli* (Figures S7F and S7G; Tables S1 and S3), suggesting that the VB12-MTR branch, which controls purine synthesis,[43,44] mediates the bacterial effect on reproductive aging.

DISCUSSION

In summary, our work discovered mtGTP-specific SCS as a key regulator of oocyte mitochondrial distribution and reproductive health, and it further identified how bacterial inputs act through mitochondrial factors to modulate reproductive longevity (Figure 7F). We found that mitochondria exhibit dispersed structure in young oocytes but undergo perinuclear clustering in aged oocytes. Interestingly, a similar age-associated change in oocyte mitochondrial distribution was also observed in mice, which has been linked to decreased Drp1 activity.[10] In our studies, we found that germline-specific overexpression of *drp-1* is sufficient to prolong RLS. In addition to its requirement for the RLS extension conferred by OP50 *E. coli* and the loss of GTP-specific SCS, DRP-1 is reported in a recent study to be necessary for the RLS extension in the *daf-2* mutant.[45] These findings together suggest that the mitochondrial fission factor DRP-1 may act downstream of multiple mechanisms and plays an evolutionarily conserved role in regulating reproductive health during aging.
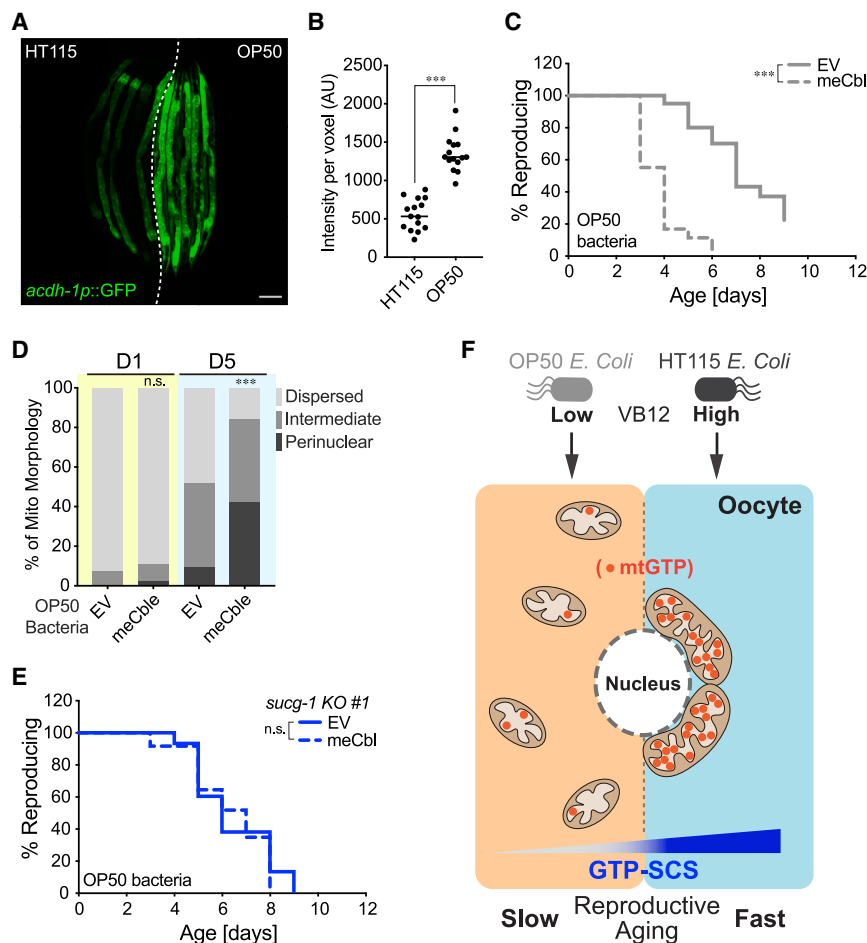
Figure 7. Bacterial VB12 regulates oocyte mitochondria and reproductive aging

(A and B) As a VB12-deficiency reporter, the *acdh-1:gfp* signal level is higher in day-1 worms on OP50 than those on HT115 bacteria. Scale bars, 100 μm in (A). GFP signal quantification is shown in (B). a.u., arbitrary unit.

(C) Supplementation of meCbl shortens RLS of WT worms on OP50 bacteria.

(D) Supplementation of meCbl increases the perinuclear clustering of oocyte mitochondria in WT worms on OP50 bacteria at day 5.

(E) Supplementation of meCbl does not shorten RLS of the *sucg-1* knockout worms on OP50 bacteria.

(F) Summary model representing mitochondrial GTP metabolism and mitochondrial fission-fusion couple in the oocyte to regulate reproductive longevity, which is modulated by metabolic inputs from bacteria.

(B) n = 15 (HT115) and n = 15 (OP50); ***p < 0.001 by Student's t test. (C) ***p < 0.001 by log rank test; n = 3 biological independent replicates, ~20 worms per replicate, see Table S3 for full RLS data. (D) n = 40 (EV, day 1), n = 45 (128 nM meCbl, day 1), n = 42 (EV, day 5), and n = 38 (128 nM meCbl, day 5); OP50 condition; 128 nM meCbl vs. EV, n.s. p > 0.05 and ***p < 0.001 by chi-squared test. (E) n.s. p > 0.05 by log rank test; n = 3 biological independent replicates, ~80 worms per replicate split into 3 genotypes, see Table S3 for full RLS data.

It is important to note that although most studies related to mitochondrial fission-fusion factors focus on mitochondrial morphology (tubular vs. fragmented), their regulation of mitochondrial distribution has been observed in both oocytes and somatic cells.[10,11,46–51] Now, our data support that the key role of mitochondrial fission-fusion factors in regulating reproductive aging is predominantly attributed to their control of mitochondrial positioning in oocytes. Perinuclear clustered mitochondria have been associated with various cellular stress.[52–58] Transient perinuclear clustering may help elicit transcriptional responses[52] and sequester damaged mitochondria[59] to restore mitochondrial homeostasis. However, prolonged perinuclear clustering of oocyte mitochondria in aged worms and mice could block mitophagy-mediated clearance of damaged mitochondria, increase ER-mitochondria aggregation to impair calcium homeostasis, as well as disrupt mitochondrial segregation required for cell division upon fertilization. Our studies provide direct evidence that the dietary and genetic interventions that drive mitochondrial dispersion from perinuclear clustering sufficiently promote reproductive longevity in worms. It would be interesting to test whether similar mechanisms could help improve reproductive health during aging in mammals.

Our studies also identified that mitochondrial metabolism may directly signal through mitochondrial fission-fusion factors. SCS locates in the mitochondrial matrix, likely to be very close to the mitochondrial inner membrane. It is reported that various enzymes in the TCA cycle interact closely and form a metabolon to facilitate their reactions.[60] One of these enzymes, succinate dehydrogenase, is anchored in the mitochondrial inner membrane.[61] Given that SCS provides succinate for succinate dehydrogenase as a substrate, the interaction between these two enzymes may recruit SCS close to the inner membrane, leading to a high local GTP level when the TCA cycle is active. Interestingly, it was reported that IMM fusion requires a higher concentration of GTP than outer mitochondrial fusion.[62] Furthermore, members of another family of GTP-producing enzymes, nucleoside diphosphate kinases, have been shown to directly interact with OPA1 in the mitochondrial inner membrane to regulate mitochondrial membrane dynamics in human cells.[30,63] Our studies found that the germline loss of EAT-3/OPA1, but not FZO-1/MFN1/2, recapitulates the effect of the germline loss of SUCG-1 in promoting reproductive longevity. Considering the age-associated increase in the germline SUCG-1 level, it is possible that an increase in GTP production close to the inner membrane drives mitochondrial fusion via EAT-3 during reproductive aging, and this imbalance of mitochondrial dynamics consequently contributes to the decline of oocyte quality.

Two recent studies discovered that MTR loss results in decreased GTP and ATP levels.[43,44] Thus, we speculate that high VB12 in HT115 *E. coli* could lead to MTR-mediated induction of GTP synthesis in the cytosol and, in turn, increased mtGTP levels. Consistently, the germline mtGTP level is

significantly greater in worms on HT115 *E. coli*. At present, we do not have direct evidence on how bacteria-derived VB12 modulates GTP-specific SCS in the reproductive system, aside from genetic analysis confirming the requirement of SUCG-1 for the effect of VB12. No mRNA or protein level difference was detected between OP50 and HT115 conditions. It is possible that VB12 influences the activity and/or substrate availability of GTP-specific SCS in oocyte mitochondria. In addition, MTR reduction also affects the level of methionine and/or homocysteine, which may also act through mitochondria to regulate reproductive aging.

We discovered that low bacterial VB12 levels are associated with reproductive longevity. There are significant variations in VB12 levels among different bacterial species. Bacteria with high or low levels of VB12 have been associated with decreased fertility in *C. elegans*.[39,40,64] In humans, a high maternal VB12 level at birth is associated with an increased risk of developing autism spectrum disorder in children.[65] However, VB12 deficiency can lead to adverse maternal and child health problems.[66,67] Thus, there may be an antagonistic pleiotropy-like effect at the nutrient level, wherein VB12 is essential for appropriate development of the germ line and progenies but later accelerates reproductive decline during aging. Our study suggests that environmental inputs from the microbiota should also be taken into account when considering this antagonistic pleiotropic effect.

Limitations of the study

We utilized the strain DCL569 to perform germline-specific RNAi KD and the *pie-1* promoter to drive germline-specific overexpression, which did not specifically target oocytes and therefore limited our investigation into oocyte-specific processes. Additionally, due to technical limitations, we were unable to track mitochondrial distribution at all stages of oocyte maturation and to capture detailed images of mitochondrial outer and inner membrane dynamics at high spatial resolution.

STAR★METHODS

Detailed methods are provided in the online version of this paper and include the following:

- KEY RESOURCES TABLE
- RESOURCE AVAILABILITY
  - Lead contact
  - Materials availability
  - Data and code availability
- EXPERIMENTAL MODEL AND STUDY PARTICIPANT DETAILS
  - Strains and maintenance
  - Strain generation – Extrachromosomal array
  - Strain Generation – Integration of extrachromosomal array
  - Strain Generation – CRISPR-Cas9 mediated insertion and deletion
  - Strain Generation – Crossing
- METHOD DETAILS
  - RNA interference (RNAi) experiments
  - Construction of plasmid and fusion PCR product
  - Reproductive lifespan assay and progeny number measurement
  - Late fertility assay
  - Confocal imaging
  - Fluorescent intensity profiling of SUCG-1::eGFP and *acdh-1p*::GFP
  - Analysis of oocyte mitochondrial network
  - mtDNA levels measurement by quantitative PCR (qPCR) and droplet digital PCR (ddPCR)
  - Body length measurement
  - Pharyngeal pumping measurement
  - Auxin treatment
  - Germline mitochondrial GTP and ATP measurement
  - Cobalamin treatment
  - Succinate treatment
  - Lifespan assay
- QUANTIFICATION AND STATISTICAL ANALYSIS

AUTHOR CONTRIBUTIONS

Y.-T.L., J.N.S., and M.C.W. conceived the project. Y.-T.L., M. Savini, T.C., J.Y., Q.Z., L.D., M. Senturk, and J.N.S. performed experiments. T.C. and S.M.G. wrote the code for imaging analysis. Y.-T.L. and M.C.W. wrote the manuscript. Y.-T.L., J.D.W., and M.C.W. edited the manuscript.

REFERENCES

1. Hamilton, B., Martin, J., and Osterman, M. (2021). Births: Provisional Data for 2020 (National Center for Health Statistics). https://doi.org/10.15620/cdc:104993.

2. Duncan, F.E., and Gerton, J.L. (2018). Mammalian oogenesis and female reproductive aging. Aging (Albany, NY) 10, 162–163. https://doi.org/10.18632/aging.101381.

3. te Velde, E.R., and Pearson, P.L. (2002). The variability of female reproductive ageing. Hum. Reprod. Update 8, 141–154. https://doi.org/10.1093/humupd/8.2.141.

4. Babayev, E., and Seli, E. (2015). Oocyte mitochondrial function and reproduction. Curr. Opin. Obstet. Gynecol. 27, 175–181. https://doi.org/10.1097/GCO.0000000000000164.

5. May-Panloup, P., Boguenet, M., El Hachem, H.E., Bouet, P.E., and Reynier, P. (2021). Embryo and its mitochondria. Antioxidants (Basel) 10, 139. https://doi.org/10.3390/antiox10020139.

6. Wilding, M., Dale, B., Marino, M., di Matteo, L., Alviggi, C., Pisaturo, M.L., Lombardi, L., and De Placido, G. (2001). Mitochondrial aggregation patterns and activity in human oocytes and preimplantation embryos. Hum. Reprod. 16, 909–917. https://doi.org/10.1093/humrep/16.5.909.

7. Reynier, P., May-Panloup, P., Chrétien, M.F., Morgan, C.J., Jean, M., Savagner, F., Barrière, P., and Malthièry, Y. (2001). Mitochondrial DNA content affects the fertilizability of human oocytes. Mol. Hum. Reprod. 7, 425–429. https://doi.org/10.1093/molehr/7.5.425.

8. Van Blerkom, J., Davis, P.W., and Lee, J. (1995). ATP content of human oocytes and developmental potential and outcome after in-vitro fertilization and embryo transfer. Hum. Reprod. 10, 415–424. https://doi.org/10.1093/oxfordjournals.humrep.a135954.

9. Detmer, S.A., and Chan, D.C. (2007). Functions and dysfunctions of mitochondrial dynamics. Nat. Rev. Mol. Cell Biol. 8, 870–879. https://doi.org/10.1038/nrm2275.

10. Udagawa, O., Ishihara, T., Maeda, M., Matsunaga, Y., Tsukamoto, S., Kawano, N., Miyado, K., Shitara, H., Yokota, S., Nomura, M., et al. (2014). Mitochondrial fission factor Drp1 maintains oocyte quality via dynamic rearrangement of multiple organelles. Curr. Biol. 24, 2451–2458. https://doi.org/10.1016/j.cub.2014.08.060.

11. Wakai, T., Harada, Y., Miyado, K., and Kono, T. (2014). Mitochondrial dynamics controlled by mitofusins define organelle positioning and movement during mouse oocyte maturation. Mol. Hum. Reprod. 20, 1090–1100. https://doi.org/10.1093/molehr/gau064.

12. Hou, X., Zhu, S., Zhang, H., Li, C., Qiu, D., Ge, J., Guo, X., and Wang, Q. (2019). Mitofusin1 in oocyte is essential for female fertility. Redox Biol. 21, 101110. https://doi.org/10.1016/j.redox.2019.101110.

13. Zhang, M., Bener, M.B., Jiang, Z., Wang, T., Esencan, E., Scott, R., III, Horvath, T., and Seli, E. (2019). Mitofusin 1 is required for female fertility and to maintain ovarian follicular reserve. Cell Death Dis. 10, 560. https://doi.org/10.1038/s41419-019-1799-3.

14. Han, B., Sivaramakrishnan, P., Lin, C.-C.J., Neve, I.A.A., He, J., Tay, L.W.R., Sowa, J.N., Sizovs, A., Du, G., Wang, J., et al. (2017). Microbial genetic composition tunes Host Longevity. Cell 169, 1249–1262.e13. https://doi.org/10.1016/j.cell.2017.05.036.

15. Weir, H.J., Yao, P., Huynh, F.K., Escoubas, C.C., Goncalves, R.L., Burkewitz, K., Laboy, R., Hirschey, M.D., and Mair, W.B. (2017). Dietary restriction and AMPK increase lifespan via mitochondrial network and peroxisome remodeling. Cell Metab. 26, 884–896.e5. https://doi.org/10.1016/j.cmet.2017.09.024.

16. Scharf, A., Pohl, F., Egan, B.M., Kocsisova, Z., and Kornfeld, K. (2021). Reproductive aging in Caenorhabditis elegans: from molecules to ecology. Front. Cell Dev. Biol. 9, 718522. https://doi.org/10.3389/fcell.2021.718522.

17. Sowa, J.N., Mutlu, A.S., Xia, F., and Wang, M.C. (2015). Olfaction modulates reproductive plasticity through neuroendocrine signaling in Caenorhabditis elegans. Curr. Biol. 25, 2284–2289. https://doi.org/10.1016/j.cub.2015.07.023.

18. Wang, M.C., Oakley, H.D., Carr, C.E., Sowa, J.N., and Ruvkun, G. (2014). Gene pathways that delay Caenorhabditis elegans reproductive senescence. PLoS Genet. 10, e1004752. https://doi.org/10.1371/journal.pgen.1004752.

19. Martínez-Reyes, I., and Chandel, N.S. (2020). Mitochondrial TCA cycle metabolites control physiology and disease. Nat. Commun. 11, 102. https://doi.org/10.1038/s41467-019-13668-3.

20. Johnson, J.D., Muhonen, W.W., and Lambeth, D.O. (1998). Characterization of the ATP- and GTP-specific succinyl-CoA synthetases in pigeon: the ENZYMES INCORPORATE THE SAME α-SUBUNIT *. J. Biol. Chem. 273, 27573–27579. https://doi.org/10.1074/jbc.273.42.27573.

21. Fraser, M.E., Hayakawa, K., Hume, M.S., Ryan, D.G., and Brownie, E.R. (2006). Interactions of GTP with the ATP-grasp domain of GTP-specific succinyl-CoA synthetase. J. Biol. Chem. 281, 11058–11065. https://doi.org/10.1074/jbc.M511785200.

22. Zou, L., Wu, D., Zang, X., Wang, Z., Wu, Z., and Chen, D. (2019). Construction of a germline-specific RNAi tool in C. elegans. Sci. Rep. 9, 2354. https://doi.org/10.1038/s41598-019-38950-8.

23. Hughes, S.E., Evason, K., Xiong, C., and Kornfeld, K. (2007). Genetic and pharmacological factors that influence reproductive aging in nematodes. PLoS Genet. 3, e25. https://doi.org/10.1371/journal.pgen.0030025.

24. Gems, D., Sutton, A.J., Sundermeyer, M.L., Albert, P.S., King, K.V., Edgley, M.L., Larsen, P.L., and Riddle, D.L. (1998). Two pleiotropic classes of daf-2 mutation affect larval arrest, adult behavior, reproduction and longevity in Caenorhabditis elegans. Genetics 150, 129–155. https://doi.org/10.1093/genetics/150.1.129.

25. Ng, L.T., Ng, L.F., Tang, R.M.Y., Barardo, D., Halliwell, B., Moore, P.K., and Gruber, J. (2020). Lifespan and healthspan benefits of exogenous H2S in C. elegans are independent from effects downstream of eat-2 mutation. NPJ Aging Mech. Dis. 6, 6. https://doi.org/10.1038/s41514-020-0044-8.

26. Luo, S., Shaw, W.M., Ashraf, J., and Murphy, C.T. (2009). TGF-beta Sma/Mab signaling mutations uncouple reproductive aging from somatic aging. PLoS Genet. 5, e1000789. https://doi.org/10.1371/journal.pgen.1000789.

27. Lakowski, B., and Hekimi, S. (1998). The genetics of caloric restriction in Caenorhabditis elegans. Proc. Natl. Acad. Sci. USA 95, 13091–13096. https://doi.org/10.1073/pnas.95.22.13091.

28. Kenyon, C., Chang, J., Gensch, E., Rudner, A., and Tabtiang, R. (1993). A C. elegans mutant that lives twice as long as wild type. Nature 366, 461–464. https://doi.org/10.1038/366461a0.

29. Fan, X., De Henau, S., Feinstein, J., Miller, S.I., Han, B., Frøkjær-Jensen, C., and Griffin, E.E. (2020). SapTrap assembly of Caenorhabditis elegans MosSCI transgene vectors. G3 (Bethesda) 10, 635–644. https://doi.org/10.1534/g3.119.400822.

30. Boissan, M., Montagnac, G., Shen, Q., Griparic, L., Guitton, J., Romao, M., Sauvonnet, N., Lagache, T., Lascu, I., Raposo, G., et al. (2014). Membrane trafficking. Nucleoside diphosphate kinases fuel dynamin superfamily proteins with GTP for membrane remodeling. Science 344, 1510–1515. https://doi.org/10.1126/science.1253768.

31. Westermann, B. (2010). Mitochondrial dynamics in model organisms: what yeasts, worms and flies have taught us about fusion and fission of mitochondria. Semin. Cell Dev. Biol. 21, 542–549. https://doi.org/10.1016/j.semcdb.2009.12.003.

32. Kanazawa, T., Zappaterra, M.D., Hasegawa, A., Wright, A.P., Newman-Smith, E.D., Buttle, K.F., McDonald, K., Mannella, C.A., and Bliek, A.M. van der (2008). The C. elegans Opa1 homologue EAT-3 is essential for resistance to free radicals. PLoS Genet. 4, e1000022. https://doi.org/10.1371/journal.pgen.1000022.

33. Ichishita, R., Tanaka, K., Sugiura, Y., Sayano, T., Mihara, K., and Oka, T. (2008). An RNAi screen for mitochondrial proteins required to maintain the morphology of the organelle in Caenorhabditis elegans. J. Biochem. 143, 449–454. https://doi.org/10.1093/jb/mvm245.

34. Avery, L. (1993). The genetics of feeding in Caenorhabditis elegans. Genetics 133, 897–917. https://doi.org/10.1093/genetics/133.4.897.

35. Breckenridge, D.G., Kang, B.-H., Kokel, D., Mitani, S., Staehelin, L.A., and Xue, D. (2008). Caenorhabditis elegans drp-1 and fis-2 regulate distinct cell-death execution pathways downstream of ced-3 and independent

of ced-9. Mol. Cell *31*, 586–597. https://doi.org/10.1016/j.molcel.2008.07.015.

36. Tan, F.J., Husain, M., Manlandro, C.M., Koppenol, M., Fire, A.Z., and Hill, R.B. (2008). CED-9 and mitochondrial homeostasis in C. elegans muscle. J. Cell Sci. *121*, 3373–3382. https://doi.org/10.1242/jcs.032904.

37. Lowry, J., Yochem, J., Chuang, C.-H., Sugioka, K., Connolly, A.A., and Bowerman, B. (2015). High-throughput cloning of temperature-sensitive Caenorhabditis elegans mutants with adult syncytial germline membrane architecture defects. G3 (Bethesda) *5*, 2241–2255. https://doi.org/10.1534/g3.115.021451.

38. Zhang, L., Ward, J.D., Cheng, Z., and Dernburg, A.F. (2015). The auxin-inducible degradation (AID) system enables versatile conditional protein depletion in C. elegans. Development *142*, 4374–4384. https://doi.org/10.1242/dev.129635.

39. Watson, E., MacNeil, L.T., Ritter, A.D., Yilmaz, L.S., Rosebrock, A.P., Caudy, A.A., and Walhout, A.J.M. (2014). Interspecies systems biology uncovers metabolites affecting C. elegans gene expression and life history traits. Cell *156*, 759–770. https://doi.org/10.1016/j.cell.2014.01.047.

40. MacNeil, L.T., Watson, E., Arda, H.E., Zhu, L.J., and Walhout, A.J.M. (2013). Diet-induced developmental acceleration independent of TOR and insulin in C. elegans. Cell *153*, 240–252. https://doi.org/10.1016/j.cell.2013.02.049.

41. Wei, W., and Ruvkun, G. (2020). Lysosomal activity regulates Caenorhabditis elegans mitochondrial dynamics through vitamin B12 metabolism. Proc. Natl. Acad. Sci. USA *117*, 19970–19981. https://doi.org/10.1073/pnas.2008021117.

42. Revtovich, A.V., Lee, R., and Kirienko, N.V. (2019). Interplay between mitochondria and diet mediates pathogen and stress resistance in Caenorhabditis elegans. PLoS Genet. *15*, e1008011. https://doi.org/10.1371/journal.pgen.1008011.

43. Ghergurovich, J.M., Xu, X., Wang, J.Z., Yang, L., Ryseck, R.-P., Wang, L., and Rabinowitz, J.D. (2021). Methionine synthase supports tumour tetrahydrofolate pools. Nat. Metab. *3*, 1512–1520. https://doi.org/10.1038/s42255-021-00465-w.

44. Sullivan, M.R., Darnell, A.M., Reilly, M.F., Kunchok, T., Joesch-Cohen, L., Rosenberg, D., Ali, A., Rees, M.G., Roth, J.A., Lewis, C.A., et al. (2021). Methionine synthase is essential for cancer cell proliferation in physiological folate environments. Nat. Metab. *3*, 1500–1511. https://doi.org/10.1038/s42255-021-00486-5.

45. Cota, V., Sohrabi, S., Kaletsky, R., and Murphy, C.T. (2022). Oocyte mitophagy is critical for extended reproductive longevity. PLoS Genet. *18*, e1010400. https://doi.org/10.1371/journal.pgen.1010400.

46. Baixauli, F., Martín-Cófreces, N.B., Morlino, G., Carrasco, Y.R., Calabia-Linares, C., Veiga, E., Serrador, J.M., and Sánchez-Madrid, F. (2011). The mitochondrial fission factor dynamin-related protein 1 modulates T-cell receptor signalling at the immune synapse. EMBO J. *30*, 1238–1250. https://doi.org/10.1038/emboj.2011.25.

47. Hennings, T.G., Chopra, D.G., DeLeon, E.R., VanDeusen, H.R., Sesaki, H., Merrins, M.J., and Ku, G.M. (2018). In vivo deletion of β-cell Drp1 impairs insulin secretion without affecting islet oxygen consumption. Endocrinology *159*, 3245–3256. https://doi.org/10.1210/en.2018-00445.

48. Pich, S., Bach, D., Briones, P., Liesa, M., Camps, M., Testar, X., Palacín, M., and Zorzano, A. (2005). The Charcot-Marie-Tooth type 2A gene product, Mfn2, up-regulates fuel oxidation through expression of OXPHOS system. Hum. Mol. Genet. *14*, 1405–1415. https://doi.org/10.1093/hmg/ddi149.

49. Shen, T., Zheng, M., Cao, C., Chen, C., Tang, J., Zhang, W., Cheng, H., Chen, K.-H., and Xiao, R.-P. (2007). Mitofusin-2 is a major determinant of oxidative stress-mediated heart muscle cell apoptosis. J. Biol. Chem. *282*, 23354–23361. https://doi.org/10.1074/jbc.M702657200.

50. Rojo, M., Legros, F., Chateau, D., and Lombès, A. (2002). Membrane topology and mitochondrial targeting of mitofusins, ubiquitous mammalian homologs of the transmembrane GTPase Fzo. J. Cell Sci. *115*, 1663–1674. https://doi.org/10.1242/jcs.115.8.1663.

51. Santel, A., and Fuller, M.T. (2001). Control of mitochondrial morphology by a human mitofusin. J. Cell Sci. *114*, 867–874. https://doi.org/10.1242/jcs.114.5.867.

52. Al-Mehdi, A.-B., Pastukh, V.M., Swiger, B.M., Reed, D.J., Patel, M.R., Bardwell, G.C., Pastukh, V.V., Alexeyev, M.F., and Gillespie, M.N. (2012). Perinuclear mitochondrial clustering creates an oxidant-rich nuclear domain required for hypoxia-induced transcription. Sci. Signal. *5*, ra47. https://doi.org/10.1126/scisignal.2002712.

53. Agarwal, S., and Ganesh, S. (2020). Perinuclear mitochondrial clustering, increased ROS levels, and HIF1 are required for the activation of HSF1 by heat stress. J. Cell Sci. *133*, jcs245589. https://doi.org/10.1242/jcs.245589.

54. Kim, S., Kim, H.-Y., Lee, S., Kim, S.W., Sohn, S., Kim, K., and Cho, H. (2007). Hepatitis B virus x protein induces perinuclear mitochondrial clustering in microtubule- and Dynein-dependent manners. J. Virol. *81*, 1714–1726. https://doi.org/10.1128/JVI.01863-06.

55. Hu, M., Schulze, K.E., Ghildyal, R., Henstridge, D.C., Kolanowski, J.L., New, E.J., Hong, Y., Hsu, A.C., Hansbro, P.M., Wark, P.A., et al. (2019). Respiratory syncytial virus co-opts host mitochondrial function to favour infectious virus production. eLife *8*, e42448. https://doi.org/10.7554/eLife.42448.

56. Pucci, B., Bertani, F., Karpinich, N.O., Indelicato, M., Russo, M.A., Farber, J.L., and Tafani, M. (2008). Detailing the role of Bax translocation, cytochrome c release, and perinuclear clustering of the mitochondria in the killing of HeLa cells by TNF. J. Cell. Physiol. *217*, 442–449. https://doi.org/10.1002/jcp.21513.

57. Dewitt, D.A., Hurd, J.A., Fox, N., Townsend, B.E., Griffioen, K.J.S., Ghribi, O., and Savory, J. (2006). Peri-nuclear clustering of mitochondria is triggered during aluminum maltolate induced apoptosis. J. Alzheimers Dis. *9*, 195–205. https://doi.org/10.3233/jad-2006-9211.

58. Thomas, W.D., Zhang, X.D., Franco, A.V., Nguyen, T., and Hersey, P. (2000). TNF-related apoptosis-inducing ligand-induced apoptosis of melanoma is associated with changes in mitochondrial membrane potential and perinuclear clustering of mitochondria. J. Immunol. *165*, 5612–5620. https://doi.org/10.4049/jimmunol.165.10.5612.

59. Geisler, S., Holmström, K.M., Skujat, D., Fiesel, F.C., Rothfuss, O.C., Kahle, P.J., and Springer, W. (2010). PINK1/Parkin-mediated mitophagy is dependent on VDAC1 and p62/SQSTM1. Nat. Cell Biol. *12*, 119–131. https://doi.org/10.1038/ncb2012.

60. Bulutoglu, B., Garcia, K.E., Wu, F., Minteer, S.D., and Banta, S. (2016). Direct evidence for metabolon formation and substrate channeling in recombinant TCA cycle enzymes. ACS Chem. Biol. *11*, 2847–2853. https://doi.org/10.1021/acschembio.6b00523.

61. Hatefi, Y. (1978). Resolution of complex II and isolation of succinate dehydrogenase (EC 1.3.99.1). In Methods in Enzymology Biomembranes - Part D: Biological Oxidations, S. Fleischer and L. Packer, eds. (Academic Press), pp. 27–35. https://doi.org/10.1016/S0076-6879(78)53009-7.

62. Meeusen, S., McCaffery, J.M., and Nunnari, J. (2004). Mitochondrial fusion intermediates revealed in vitro. Science *305*, 1747–1752. https://doi.org/10.1126/science.1100612.

63. Schlattner, U., Tokarska-Schlattner, M., Ramirez, S., Tyurina, Y.Y., Amoscato, A.A., Mohammadyani, D., Huang, Z., Jiang, J., Yanamala, N., Seffouh, A., et al. (2013). Dual function of mitochondrial Nm23-H4 protein in phosphotransfer and intermembrane lipid transfer: a cardiolipin-dependent switch. J. Biol. Chem. *288*, 111–121. https://doi.org/10.1074/jbc.M112.408633.

64. Qin, S., Wang, Y., Li, L., Liu, J., Xiao, C., Duan, D., Hao, W., Qin, C., Chen, J., Yao, L., et al. (2022). Early-life vitamin B12 orchestrates lipid peroxidation to ensure reproductive success via SBP-1/SREBP1 in Caenorhabditis elegans. Cell Rep. *40*, 111381. https://doi.org/10.1016/j.celrep.2022.111381.

65. Raghavan, R., Riley, A.W., Volk, H., Caruso, D., Hironaka, L., Sices, L., Hong, X., Wang, G., Ji, Y., Brucato, M., et al. (2018). Maternal multivitamin intake, plasma folate and vitamin B12 levels and autism spectrum disorder

risk in offspring. Paediatr. Perinat. Epidemiol. *32*, 100–111. https://doi.org/10.1111/ppe.12414.

66. Molloy, A.M., Kirke, P.N., Brody, L.C., Scott, J.M., and Mills, J.L. (2008). Effects of folate and vitamin B12 deficiencies during pregnancy on fetal, infant, and child development. discussion S112–S115. Food Nutr. Bull. *29*, S101–S111. https://doi.org/10.1177/15648265080292S114.

67. Green, R., Allen, L.H., Bjørke-Monsen, A.-L., Brito, A., Guéant, J.-L., Miller, J.W., Molloy, A.M., Nexo, E., Stabler, S., Toh, B.-H., et al. (2017). Vitamin B12 deficiency. Nat. Rev. Dis. Primers *3*, 17040. https://doi.org/10.1038/nrdp.2017.40.

68. Neve, I.A.A., Sowa, J.N., Lin, C.-C.J., Sivaramakrishnan, P., Herman, C., Ye, Y., Han, L., and Wang, M.C. (2020). Escherichia coli metabolite profiling leads to the development of an RNA interference strain for Caenorhabditis elegans. G3 (Bethesda) *10*, 189–198. https://doi.org/10.1534/g3.119.400741.

69. Dokshin, G.A., Ghanta, K.S., Piscopo, K.M., and Mello, C.C. (2018). Robust genome editing with short single-stranded and long, partially single-stranded DNA donors in Caenorhabditis elegans. Genetics *210*, 781–787. https://doi.org/10.1534/genetics.118.301532.

70. Chen, X., Xu, F., Zhu, C., Ji, J., Zhou, X., Feng, X., and Guang, S. (2014). Dual sgRNA-directed gene knockout using CRISPR/Cas9 technology in Caenorhabditis elegans. Sci. Rep. *4*, 7581. https://doi.org/10.1038/srep07581.

71. Rual, J.-F., Ceron, J., Koreth, J., Hao, T., Nicot, A.-S., Hirozane-Kishikawa, T., Vandenhaute, J., Orkin, S.H., Hill, D.E., van den Heuvel, S., et al. (2004). Toward improving Caenorhabditis elegans phenome mapping with an ORFeome-based RNAi library. Genome Res. *14*, 2162–2168. https://doi.org/10.1101/gr.2505604.

72. Kamath, R.S., and Ahringer, J. (2003). Genome-wide RNAi screening in Caenorhabditis elegans. Methods *30*, 313–321. https://doi.org/10.1016/S1046-2023(03)00050-1.

73. Gervaise, A.L., and Arur, S. (2016). Spatial and temporal analysis of active ERK in the C. elegans Germline. J. Vis. Exp.54901 https://doi.org/10.3791/54901.

74. Ahier, A., Dai, C.-Y., Tweedie, A., Bezawork-Geleta, A., Kirmes, I., and Zuryn, S. (2018). Affinity purification of cell-specific mitochondria from whole animals resolves patterns of genetic mosaicism. Nat. Cell Biol. *20*, 352–360. https://doi.org/10.1038/s41556-017-0023-x.

75. Fung, D.K., Yang, J., Stevenson, D.M., Amador-Noguez, D., and Wang, J.D. (2020). Small alarmone synthetase SasA expression leads to concomitant accumulation of pGpp, ppApp, and AppppA in Bacillus subtilis. Front. Microbiol. *11*, 2083. https://doi.org/10.3389/fmicb.2020.02083.

76. Yang, J., Anderson, B.W., Turdiev, A., Turdiev, H., Stevenson, D.M., Amador-Noguez, D., Lee, V.T., and Wang, J.D. (2020). The nucleotide pGpp acts as a third alarmone in Bacillus, with functions distinct from those of (p) ppGpp. Nat. Commun. *11*, 5388. https://doi.org/10.1038/s41467-020-19166-1.

77. Clasquin, M.F., Melamud, E., and Rabinowitz, J.D. (2012). LC-MS data processing with MAVEN: a metabolomic analysis and visualization engine. Curr. Protoc. Bioinformatics *Chapter 14*, Unit14.11. https://doi.org/10.1002/0471250953.bi1411s37.

STAR★METHODS

KEY RESOURCES TABLE

REAGENT or RESOURCE	SOURCE	IDENTIFIER
Bacterial and Virus Strains		
Escherichia coli HT115(DE3)	Caenorhabditis Genetics Center	HT115
Escherichia coli OP50	Caenorhabditis Genetics Center	OP50
Escherichia coli HB101	Caenorhabditis Genetics Center	HB101
Vidal RNAi library	Open Biosystems	ORF RNAi Collection V1.1
Ahringer RNAi library	Source BioScience	*C. elegans* RNAi Collection (Ahringer)
RNA interference competent OP50 strain (*rnc:14::DTn10; laczgA::T7pol camFRT*)	Neve et al.[68]	N/A
Experimental Models: Organisms/Strains		
C. elegans N2 Wild-type	Caenorhabditis Genetics Center	N2 (RRID:WB-STRAIN:WBStrain00000001)
sucg-1(syb3617[sucg-1::eGFP]) IV	Suny Biotech	PHX3617
suca-1(syb4685[suca-1::eGFP]) X	Suny Biotech	PHX4685
mkcSi13[sun-1p::rde-1::sun-1 3'UTR + unc-119(+)] II; rde-1(mkc36) V	Caenorhabditis Genetics Center	DCL569 (RRID:WB-STRAIN:WBStrain00005607)
egxSi155[mex-5p:tomm-20::mKate2::pie-1 3'UTR + unc-119(+)] II; unc-119(ed3) III	Caenorhabditis Genetics Center	EGD629
egxSi155[mex-5p:tomm-20::mKate2::pie-1 3'UTR + unc-119(+)] II; unc-119(ed3) III; sucg-1(syb3617[sucg-1::eGFP]) IV	This paper	MCW1373
raxEx618[pie-1p::cox8(MTS)::ndk-1::3xHA::pie-1 3'UTR + myo-2p::GFP]	This paper	MCW1581
egxSi152[mex-5p: tomm-20::gfp::pie-1 3'UTR + unc-119(+)] II; unc-119(ed3) III	Caenorhabditis Genetics Center	EGD623
raxEx190[pie-1p::drp-1::tbb-2 3'UTR + myo-2p::GFP]	This paper	MCW618
raxIs141[pie-1p::drp-1::tbb-2 3'UTR + myo-2p::GFP]	This paper	MCW1220
raxIs141[pie-1p::drp-1.b::tbb-2 3'UTR + myo-2p::GFP]; egxSi152[mex5p::tomm-20::gfp::pie-1 3'UTR + unc-119(+)] II; unc-119(ed3) III	This paper	MCW1357
drp-1(or1941[GFP::drp-1]) IV	Caenorhabditis Genetics Center	EU2917 (RRID:WB-STRAIN:WBStrain00007414)
drp-1(rax82[GFP::Degron::drp-1]) IV	This paper	MCW1315
ieSi68[sun-1p::TIR1::mRuby::htp-1 3'UTR + Cbr-unc-119(+)] II; unc-119(ed3) III	Caenorhabditis Genetics Center	CA1472 (RRID:WB-STRAIN:WBStrain00004073)
ieSi68[sun-1p::TIR1::mRuby::htp-1 3'UTR + Cbr-unc-119(+)] II; unc-119(ed3) III; drp-1(rax82[GFP::Degron::drp-1]) IV	This paper	MCW1326
drp-1(tm1108) IV	Caenorhabditis Genetics Center	CU6372 (RRID:WB-STRAIN:WBStrain00005196)
egxSi152[mex5p::tomm-20::GFP::pie-1 3'UTR + unc-119(+)] II; unc-119(ed3) III; drp-1(tm1108) IV	This paper	MCW1584
sucg-1(rax83) IV	This paper	MCW1325
sucg-1(rax86) IV	This paper	MCW1331
suca-1(rax84) X	This paper	MCW1329
suca-1(rax85) X	This paper	MCW1330

(Continued on next page)

Continued

REAGENT or RESOURCE	SOURCE	IDENTIFIER
sucg-1(syb3617[sucg-1::eGFP]); *sucg-1(rax83) IV*	This paper	MCW1375
sucg-1(syb3617[sucg-1::eGFP]); *sucg-1(rax86) IV*	This paper	MCW1385
raxIs89[sun-1p::eGFP::sun-1 3'UTR] III)	This paper	MCW1408
raxIs98[sun-1p::eGFP::3xHA:: *sun-1 3'UTR] III)*	This paper	MCW1473
raxIs109[sun-1p::tomm-20 *(1-55aa)::eGFP::3xHA::sun-1 3'UTR] III*	This paper	MCW1550
wwIs24 [acdh-1p::GFP + unc-119(+)]	Caenorhabditis Genetics Center	VL749 (RRID:WB-STRAIN:WBStrain00040155)
Oligonucleotides		
See Table S4 for primers used in the study	Integrated DNA Technologies	N/A
See Table S5 for crRNA and tracrRNA used in the study	Horizon Discovery Ltd.	N/A
Recombinant DNA		
pDONR221	Invitrogen	Cat# 12536017
pCM1.36	Addgene	RRID:Addgene_17249
pCM1.127	Addgene	RRID:Addgene_21384
pCFJ150	Addgene	RRID:Addgene_19329
pPK605	Addgene	RRID:Addgene_38148
Software and Algorithms		
ImageJ v1.52p	http://fiji.sc/	RRID:SCR_003070
Illustrator CC 2022	Adobe	RRID:SCR_010279
PRISM v9	GraphPad Software	RRID:SCR_002798
SPSS v24.0	IBM	RRID:SCR_016479
BioRender	https://biorender.com/	RRID:SCR_018361
MATLAB R2020a	MathWorks	RRID:SCR_001622

RESOURCE AVAILABILITY

Lead contact
Further information and requests for resources and reagents should be directed to and will be fulfilled by the lead contact, Meng C. Wang (mengwang@janelia.hhmi.org).

Materials availability
Materials including *C. elegans* strains, sequences, and plasmids in this study are available upon request.

Data and code availability
All reproductive lifespan and lifespan data are available in the paper's supplemental information. All other data reported in this paper will be shared by the lead contact upon request. All original code is available in this paper's supplemental information. Any additional information required to reanalyze the data reported in this paper is available from the lead contact upon request.

EXPERIMENTAL MODEL AND STUDY PARTICIPANT DETAILS

Strains and maintenance
C. elegans strains N2, DCL569, EGD629, EGD623, EU2917, CA1472, CU6372, and VL749 were obtained from the Caenorhabditis Genetics Center. PHX3617 and PHX4685 were acquired from Suny Biotech. MCW618, MCW1220, MCW1315, MCW1325, MCW1326, MCW1329, MCW1330, MCW1331, MW1357, MCW1373, MCW1375, MCW1385, MCW1408, MCW1473, MCW1550, MCW1581, MCW1584 were made in our lab. All *C. elegans* strains were kept at 20°C for both maintenance and experiment. All *C. elegans* were non-starved for at least 2 generations on NGM plates seeded with OP50 bacteria before any experiment. The detailed genotypes of each strain are listed in the key resources table.

The *E. coli* strain HT115 (DE3) was obtained from the Ahringer RNAi library. The *E. coli* strains OP50 and HB101 were obtained from the Caenorhabditis Genetics Center.

Strain generation – Extrachromosomal array

MCW618 (*raxEx190[pie-1p::drp-1::tbb-2 3′UTR + myo-2p::GFP]*) was generated by microinjecting the *pie-1p::drp-1::tbb-2 3′UTR* linearized PCR product and *myo-2p::GFP* plasmids into the gonad of young adults. MCW1581 (*raxEx618[pie-1p::cox8(mitochondrial targeting sequence)::ndk-1::3xHA::pie-1 3′UTR + myo-2p::GFP]*) was generated by microinjecting *pie-1p::cox8(mitochondrial targeting sequence)::ndk-1::3xHA::pie-1 3′UTR* linearized PCR product and *myo-2p::GFP* plasmid into the gonad of young adults.

Strain Generation – Integration of extrachromosomal array

MCW1220 (*raxIs141[pie-1p::drp-1::tbb-2 3′UTR + myo-2p::GFP]*) was generated by the integration of extrachromosomal array in MCW618 which is induced by gamma irradiation exposures (4500rad, 5.9min) at the L4 stage. Later, the integrated progenies were backcrossed to N2 five times.

Strain Generation – CRISPR-Cas9 mediated insertion and deletion

MCW1315 (*drp-1(rax82[GFP::Degron::drp-1]) IV*) was generated by inserting the Degron sequence into the *GFP::drp-1* locus of EU2917 between *GFP* and *drp-1* following the protocol from Dokshin et al. with some modifications.[69] In short, a mixture of Cas9 protein (1.25μg/μl), tracrRNA (1μg/μl), target crRNA (0.4μg/μl), *dpy-10* crRNA (0.16μg/μl), and partially single-stranded DNA donor (300nM final concentration for each PCR product) was microinjected into the gonad of young adults. The partially single-stranded DNA donor was generated by mixing 2 PCR products – Degron sequence with 30 or 100 base pair homology arms on each side, and heat to 95°C then gradually cooling back to 20°C for melting and reannealing. After 3 days, the plates that have worms with *Dpy* phenotype were carefully chosen as jackpot plates for individualization of non-*Dpy* worms. These worms were subjected to pooled and then individual genotyping PCR after they reproduced to ensure passage of the genotype. The progenies (F2) of the specific F1 worm with the desired genotype were further individualized for identification of homozygosity using genotyping PCR and then Sanger sequencing.

MCW1325(*sucg-1(rax83) IV*), MCW1331(*sucg-1(rax86) IV*), MCW1329(*suca-1(rax84) X*), and MCW1330(*suca-1(rax85) X*) knockout or partial knockout strains were generated using methodologies described in Chen et al. with modifications.[70] A mixture of Cas9 protein (1.25μg/μl), tracrRNA (1μg/μl), 2 target crRNAs (0.4μg/μl each) on 5′ and 3′ of a gene, and *dpy-10* crRNA (0.16μg/μl), were microinjected into the gonad of young adults. The screening process was the same as described for the knock-in strain MCW1315. MCW1329 and MCW1330 were backcrossed to N2 three times.

MCW1408 (*raxIs89[sun-1p::eGFP::sun-1 3′UTR] III*) was generated by inserting *sun-1p::eGFP::sun-1 3′UTR* into ChrIII 7007.6 position. A mixture of Cas9 protein (1.25μg/μl), tracrRNA (1μg/μl), target crRNA (0.4μg/μl), and partially single-stranded DNA donor (10nM final concentration for each PCR product) was microinjected into the gonad of young adults. The partially single-stranded DNA donor was generated by mixing 2 PCR products - *sun-1p::eGFP::sun-1 3′UTR* sequence with 150bp of flanking homology arms on each side and the plain *sun-1p::eGFP::sun-1 3′UTR* sequence (both amplified using pYT17 plasmid as template), and heat to 95°C then gradually cool back to 20°C for melting and reannealing. Each injected worms were individualized post-injection. After 4 days, F1s were screened under fluorescence scope for green fluorescence in the germline. The progenies (F2) of the specific F1 worm with the desired genotype were further individualized for identification of homozygosity using fluorescence scope and then genotyping PCR followed by Sanger sequencing.

MCW1473 (*raxIs98[sun-1p::eGFP::3xHA::sun-1 3′UTR] III*) was generated by inserting triple HA sequence between e*GFP* and *sun-1 3′UTR* at ChrIII 7007.6 position; *sun-1p::eGFP::sun-1 3′UTR* genetic locus in MCW1408. The experiment procedure was the same as generating MCW1315 except for the usage of single-strand oligodeoxynucleotides (with 30∼40nt homology arms on each side; 250ng/μl final concentration) instead of partially single-stranded DNA donor as the repair template, and melting and reannealing step by heating and cooling was not performed.

MCW1550 (*raxIs109[sun-1p::tomm-20(1-55aa)::eGFP::3xHA::sun-1 3′UTR] III*) as generated by inserting the first 165 nucleotides of *tomm-20* gene between *sun-1p* and *eGFP* at ChrIII 7007.6 position; *sun-1p::eGFP::3xHA::sun-1 3′UTR* genetic locus in MCW1473. The experiment procedure was the same as generating MCW1473. Later, MCW1550 was backcrossed to N2 five times.

Genotyping PCR was performed using spanning primers for MCW1315, MCW1325, MCW1331, MCW1329, MCW1330, and MCW1408, and then followed by confirmation with Sanger sequencing. For MCW1473 and MCW1550, genotyping PCR screen was performed using spanning primer on the 5' and internal primer on the 3', and the candidates were further verified using genotyping PCR by spanning primers followed by confirmation with Sanger sequencing.

All primers used for genotyping are listed in Table S4. Sequences of all crRNAs and the tracrRNA used for generating strains by CRISPR-Cas9 are listed in Table S5.

Strain Generation – Crossing

MCW1373 (*egxSi155[mex-5p::tomm-20::mKate2::pie-1 3′UTR + unc-119(+)] II; unc-119(ed3) III; sucg-1(syb3617[sucg-1::eGFP]) IV*) was generated by crossing PHX3617 male to EGD629 hermaphrodite. eGFP⁺ F1s were selected to a population plate under the fluorescent scope, and the eGFP⁺ F2s on the population plate were then picked into individual plates. The F3s were later examined for green fluorescence, and individual plates with all eGFP⁺ (homozygous) F3 worms were then selected. Confocal imaging was then

used to screen for the *tomm-20::mKate2* homozygous genotype, and genotyping PCR followed by Sanger sequencing were used to examine the *unc-119* genotype.

MCW1326 (*ieSi68[sun-1p::TIR1::mRuby::htp-1 3'UTR + Cbr-unc-119(+)] II; unc-119(ed3) III; drp-1(rax82[GFP::Degron::drp-1]) IV*) was generated by crossing MCW1315 male to CA1472 hermaphrodite. F1s were picked into individual plates, and then the *GFP::Degron::drp-1*; *TIR-1::mRuby* (heterozygous) genotype was inspected by confocal imaging after egg laying. The F2s from F1 with the correct heterozygous genotype were then picked into individual plates. Later, F3s were later used to screen for the correct homozygous genotype of *GFP::Degron::drp-1*; *TIR-1::mRuby* by confocal imaging. Lastly, genotyping PCR followed by Sanger sequencing were used to examine the *unc-119* genotype.

MCW1357 (*raxIs141[pie-1p::drp-1.b::tbb-2 UTR + myo-2p::GFP]; egxSi152[mex5p::tomm-20::GFP::pie-1 3'UTR + unc-119(+)] II; unc-119(ed3) III*) was generated by crossing EGD623 male to MCW1220 hermaphrodite. F1s were inspected for the *mex5p::tomm-20::GFP::pie-1 3'UTR* by the fluorescent microscope, and the worms with the correct (heterozygous) genotype were individualized. Later, the *myo-2p::GFP*⁺ F2s from F1 with the correct *mex5p::tomm-20::GFP::pie-1 3'UTR* heterozygous genotype were then picked into individual plates. Later, F3s were later used to screen for the correct homozygous genotype of *myo-2p::GFP* and *mex5p::tomm-20::GFP::pie-1 3'UTR* by fluorescence scope. Lastly, genotyping PCR followed by Sanger sequencing were used to examine the *unc-119* genotype.

MCW1584 (*egxSi152[mex5p::tomm-20::GFP::pie-1 3'UTR + unc-119(+)] II; unc-119(ed3) III; drp-1(tm1108) IV*) was generated by crossing EGD623 male to CU6372 hermaphrodite. F1s were then inspected for the *mex5p::tomm-20::GFP::pie-1 3'UTR* by the fluorescent microscope, and the ones with the correct (heterozygous) genotype were individualized. The F2s from F1 with the correct *mex5p::tomm-20::GFP::pie-1 3'UTR* heterozygous genotype were then picked into individual plates, and single worm lysed for *drp-1(tm1108)* PCR genotyping after egg laying. Later, F3s were used to screen for the correct homozygous genotype of *mex5p::tomm-20::GFP::pie-1 3'UTR* by fluorescent microscope. Lastly, genotyping PCR followed by Sanger sequencing were used to examine the *unc-119* genotype.

Genotyping PCR of for *drp-1(tm1108)* and *unc-119* was performed using spanning primers followed by confirmation with Sanger sequencing. The primers used for *drp-1(tm1108)* and *unc-119* genotyping are listed in Table S4.

MCW1375 (*sucg-1(syb3617[sucg-1::eGFP]); sucg-1(rax83) IV*) and MCW1385 (*sucg-1(syb3617[sucg-1::eGFP]); sucg-1(rax86) IV*) were obtained by crossing PHX3617 male to MCW1325 or MCW1331 hermaphrodites. eGFP⁺ F1s were picked under the fluorescent microscope and picked into individual plates. Later, F2s were used to confirm the *sucg-1*::*gfp*/KO heterozygous genotype of the F1 parental worms by fluorescent microscope (eGFP⁺/eGFP⁻ F2s should be around 3:1). Heterozygous genotypes were maintained by picked eGFP⁺ heterozygous worms (lower eGFP intensity than homozygous) for passage.

METHOD DETAILS

RNA interference (RNAi) experiments

RNAi libraries created by the lab of Dr. Marc Vidal and Dr. Julie Ahringer were used in this study.[71,72] *sucg-1, mev-1, sdhb-1, ogdh-1, drp-1, eat-3,* and *mmcm-1* RNAi clones were acquired from the Vidal library while *sucl-2, suca-1,* and *metr-1* RNAi clones were acquired from the Ahringer library. *fzo-1* RNAi clone was generated in the lab using L4440 as the vector backbone and full-length *fzo-1* transcript as the insert. All RNAi clones were verified by Sanger sequencing. For OP50 RNAi experiments, the genetically modified competent OP50 bacteria *[rnc14::DTn10 laczgA::T7pol camFRT]* generated by our lab was used and transformed with 50 ng of the RNAi plasmid every time before the experiment.[68] All RNAi colonies were selected in both 50 μg ml⁻¹ carbenicillin and 50 μg ml⁻¹ tetracycline resistance. All RNAi bacteria were cultured for 14 hours in LB with 25 μg ml⁻¹ carbenicillin, and then seeded onto RNAi agar plates that contain 1 mM IPTG and 50 μg ml⁻¹ carbenicillin. The plates were then left at room temperature overnight for induction of dsRNA expression. For the RNAi experiments that require auxin treatment, fresh bacteria were concentrated 4 times before seeding onto the plates, and then left at 4°C overnight before usage.

Construction of plasmid and fusion PCR product

The *pie-1p::drp-1::tbb2 3'UTR* plasmid was generated by PCR amplifying the complete coding sequence of *drp-1.b* transcript from N2 cDNA and utilized Gateway BP recombination to clone into pDONR221 which contains Gateway attLR recombination sequences. *drp-1.b* CDS entry clone was then recombined with the entry clones pCM1.36-*tbb-2* 3'UTR and pCM1.127-*pie-1p* into destination vector pCFJ150 using Gateway LR recombination.

The *pie-1p::cox8(mitochondrial targeting sequence)::ndk-1::3xHA::pie-1 3'UTR* oligonucleotide was generated by 3-fragment fusion PCR using *cox8(mitochondrial targeting sequence)::ndk-1::3xHA, pie-1p,* and *pie-1 3'UTR* PCR product. The *cox8(mitochondrial targeting sequence)::ndk-1::3xHA* oligonucleotide was synthesized by IDT, and utilized as the template for amplification and homology arm tagging (tagged with *pie-1p* and *pie-1 3'UTR* homologies on 5' and 3' end respectively). Both *pie-1p* and *pie-1 3'UTR* PCR products were amplified using pPK605 plasmid (Addgene) as the template.

The pYT17-*sun-1p::eGFP::sun-1 3'UTR* plasmid was generated via 4-fragment Gibson cloning from vector backbone, *sun-1p*, modified *eGFP*, and *sun-1 3'UTR* PCR products. *sun-1p* and *sun-1 3'UTR* PCR products were amplified using N2 worm lysate as the template. The modified *eGFP* PCR product was amplified using PHX3617 worm lysate as the template.

Primers used for the amplification are listed in Table S4.

Reproductive lifespan assay and progeny number measurement

Synchronized L1 larvae from egg preparation were plated onto 6cm NGM plates seeded with the specific bacteria (default: HT115) and grew to L4 stage before being individualized into single 3cm NGM plates. The worms were transferred to a new plate every day except for the day right after individualization, which we collectively (L4 + day-1-old adult) count as day 1. The transferring stopped when we observed 2 days of non-reproducing events consecutively or until day 12. After each transfer, plates were stored at room temperature for 2 days before checking the reproductive status, and counting progeny number if necessary. The last day of progeny production was counted as the day of reproductive cessation, and worms that could not be tracked until the day of reproductive cessation due to missing, death, germline protrusion, or internal hatching were counted as censors on the last day which we could determine the reproductive status. The animals were removed from the reproductive lifespan analysis if they died before producing any progeny. For total progeny number measurement, only the worms that are tracked until reproductive cessation are included.

For RLS experiments of MCW1581 *(raxEx618[pie-1p::cox8(mitochondrial targeting sequence)::ndk-1::3xHA::pie-1 3'UTR + myo-2p::GFP])*, day 1 *myo-2p*::GFP$^+$ F1s of injected parental worms were individually picked onto EV or *sucg-1* RNAi plates. 3 and 4 days later, the plates with *myo-2p*::GFP$^+$ F2s were selected, and the same number of *myo-2p*::GFP$^+$ and *myo-2p*::GFP$^-$ F2 worms at L4 stage were picked from each population plate into individual EV or *sucg-1* RNAi plates. The later part of the RLS methodology follows the protocol above.

For RLS experiments of MCW1375 and MCW1385 strains, heterozygous parental worms were individualized onto the 6cm NGM plates at day 1 adulthood and the plates were kept for 4 days. The genotypes of the parental worms were then examined by the eGFP phenotypes in F1 under the fluorescent scope to ensure heterozygosity (of the parental line), and F1 progenies at L4 stage were randomly picked and individualized onto 3cm NGM plates. The later part of the RLS methodology follows the protocol above, with an additional step of examining the genotype of each F1 worm by observing the eGFP phenotypes in F2s.

Late fertility assay

Synchronized L1 larvae from egg preparation were plated on 6cm NGM plates seeded with the specific bacteria (default: HT115) and transferred every 2 days to new NGM plates from L4 until day 9. Individual hermaphrodites were transferred to 3cm NGM plates seeded with OP50 bacteria together with 2 day-2-old young N2 males for mating. Hermaphrodites were mated for 2 days before the first round of examination, which will exclude the plates with dead hermaphrodites, germline protruded hermaphrodites, or 2 dead males. The plates were then kept for one more day until the second-round examination of progeny production. Unlike RLS, internal hatched worms were not censored but instead considered as a reproduction event in late fertility assay. 15-20 hermaphrodites were used for each experiment, which was repeated at least 3 times independently to reach 60 worms per condition (before exclusion). The results from different trials were then pooled to conduct Fisher's exact test to determine whether the number of worms that resumed reproduction after mating in each condition significantly differed from the controls.

Confocal imaging

Sample preparations were done by anesthetizing the worms in 1% sodium azide (NaAz) in M9 buffer and mounting them on 2% agarose pads on glass slides, and later covering the pads with coverslips. The worms were then imaged on laser scanning confocal FV3000 (Olympus, US) with water immersion 60x objective (UPLSAPO 60XW, Olympus, US) for SUCG-1 mitochondrial localization in the germline, germline morphology and mitochondrial localization of day 5 worms subjected to *drp-1* RNAi knockdown, and oocyte mitochondrial distribution. 20x objective (UPLSAPO 20X, Olympus, US) was used for assessing the expression pattern of SUCG-1::eGFP and SUCA-1::eGFP, and the intensity of SUCG-1::eGFP in the germline on day 1 and day 5. 10X objective (UPlanFL N 10X, Olympus, US) was used to measure the body length of worms subjected to EV or *eat-3* germline-specific RNAi knockdown, and intensity of intestinal *acdh-1p*::GFP on OP50 and HT115 bacteria.

Fluorescent intensity profiling of SUCG-1::eGFP and *acdh-1p*::GFP

The images of the germline SUCG-1::eGFP were generated by 20x z-stacked confocal imaging of PHX3617 strain, and the images of intestinal *acdh-1p*::GFP were generated by 10x z-stacked confocal imaging of VL749 strain.

For a given 3D image stack of eGFP labeled germline or intestine, the max intensity at each (x,y) location was projected to a single image, i_{max}. Multiple polygons $p_1, p_2, ..., p_m$ (m is the number of imaged germlines) were manually selected on i_{max} to outline germlines. A 2D mask m_i was generated for each p_i, with i =1, 2, ..., m. m_i was extended to 3D mask v_i by multiplying the depth of the stack and then using the v_i to select the 3D region for calculation total and average intensity of eGFP. For SUCG-1::eGFP, the region selected spans from the proliferation zone to the mid-point of the U-shaped loop due to technical difficulties in consistently getting quality images of the entire germline and the blurred border between oocyte and spermatheca in aged worms. For *acdh-1p*::GFP, the entire intestine of the worms was selected for analysis.

All analyses above were done using MATLAB. Student's test was used to determine whether the SUCG-1::eGFP intensities of day-5-old worms are statistically distinct from the day-1-old worms, and whether the *acdh-1p*::GFP intensities of worms on OP50 bacteria are statistically distinct from worms on HT115 bacteria. The code for the analyses is provided in File S1.

Analysis of oocyte mitochondrial network

The images of the oocyte mitochondrial network were generated by 60x confocal imaging of EGD623 strain or mutant and integrated strains crossed with EGD623, and the position -2 oocytes were used for downstream analysis. Stacked oocytes with little distance between the nuclear membrane and the lateral side of the plasma membrane were excluded from the analysis.

For code-based radial intensity profiling of the oocyte mitochondrial network, mitochondrial distribution as their distance from the nucleus was quantified by generating two masks using manual selection with a polygon on the images - polygon p_1 outlining the nucleus and p_2 outlining the cell body. A set of rays were calculated with their origins at the mass center of p_1. The rays were customized to cover 360° with a step size of 1°. Each ray intersected with p_1 and p_2 and got a line segment. All line segments were divided into 5 equal segments, and labeled as ls_1, ls_2, …, ls_5, starting from the segment closest to the nucleus. All ends of ls_1 were connected to get a ring shape r_1, and then the same for ls_2 to ls_5 resulting in r_2 to r_5. These rings were used as masks to select regions in an oocyte for mitochondrial intensity calculation leading to the generation of radial mitochondrial distribution. All the above analyses were done using MATLAB. The code for the analyses is provided in File S2.

Later, the ring 1 occupancy of each oocyte was converted into one of the three categories using the following cutoffs – dispersed when lower than 23.5%, intermediate when equal or higher than 23.5% but lower than 26.5%, and perinuclear when equal or higher than 26.5%. The cutoffs were defined through double-blind categorization. Chi-squared test was then used to determine whether the oocyte mitochondrial distribution of each condition is significantly different from the control.

mtDNA levels measurement by quantitative PCR (qPCR) and droplet digital PCR (ddPCR)

The protocol from Gervaise and Arur was followed for worm collection and germline dissection.[73]

For the germline mtDNA levels measurement by qPCR, around 30 germlines were dissected for each condition. After dissection, germlines in M9 solution were collected into a PCR tube with a glass Pasteur pipette and centrifuged at 15000rpm for 2 minutes. Later, the excess M9 solution was removed from the PCR tube, and worm lysis buffer was added. The PCR tube was then placed at -80°C for at least 15 minutes before incubating at 60°C for 60 minutes followed by 95°C for 15 minutes for lysis and DNA release. qPCR was then performed using Power SYBR green master mix (Applied Biosystems #4367659) in a realplex 4 qPCR cycler (Eppendorf). To calculate the relative mtDNA levels, the cycle number of *nduo-1* and *ctb-1* (both encoded by mitochondrial DNA) were normalized to *ant-1.3* (encoded by genomic DNA).

For the oocyte mtDNA copy number measurement by ddPCR, the proximal gonads containing differentiated oocytes (from -1 oocyte to where the loop/U-turn starts) were dissected. After dissection, each proximal gonad in M9 solution was collected into a PCR tube using a P2 pipette with low-retention tips, and worm lysis buffer was added. The PCR tube was then placed at -80°C for at least 15 minutes before incubating at 60°C for 60 minutes followed by 95°C for 15 minutes for lysis and DNA release. ddPCR was then performed using EvaGreen supermix (Bio-Rad #1864034) with droplet generation (Bio-Rad #1864002) followed by PCR in a thermocycler (Bio-Rad #1851196), and signals in each droplet were then detected by the droplet reader (Bio-Rad #1864003). The QX manager software was used for visualization and threshold setting to acquire droplet numbers that are positive and negative for the signal and then followed by copy number calculation using the online tool from Stilla Technologies (https://www.stillatechnologies. com/digital-pcr/statistical-tools/poisson-law-calculation/). To calculate the mtDNA copy per oocyte, the copy number of *nduo-1* and *ctb-1* were normalized to *ant-1.3*.

Body length measurement

The DIC channel on confocal microscopy was used to image the full body lengths of day 1 worms subjected to EV or *eat-3* germline-specific RNAi knockdown side by side. The images were then analyzed using ImageJ by drawing segmented lines spanning the head to tail of the worms, which was then followed by distance measurement.

Pharyngeal pumping measurement

A digital camera (ORCA-Flash4.0 LT, Hamamatsu) attached to the stereoscope was used to record the pharyngeal pumping rate of worms subjected to EV or *eat-3* germline-specific RNAi knockdown. After recording, the movies were played at 0.25X speed, and the times of pharyngeal pumping in each second (pumping rate) were counted. For each worm, the average pumping rate in 5-10 seconds was used for analysis.

Auxin treatment

Auxin (Alfa Aesar #A10556) was administered to the *C. elegans* using methodologies described in Zhang et al. with slight modification.[38] A 400mM auxin stock solution in ethanol was prepared and filtered through a 0.22μm filter, which was stored at 4°C for up to 2 weeks. Auxin stock solution was added into the NGM liquid agar with a concentration of 1 to 100 (1%) after the autoclaved liquid agar dropped below 50°C and then poured into the plates making a final auxin concentration of 4mM. For the control plates, filtered ethanol was added to the NGM liquid agar with a concentration of 1 to 100 (1%). The plates were stored at 4°C inside a box with low photopermeability after the agar solidified. Before usage, fresh bacteria were concentrated by 4X before seeding onto the plates, and the plates that weren't used immediately were stored at 4°C for up to 5 days.

Germline mitochondrial GTP and ATP measurement

Synchronized MCW1550 L1 larvae from egg preparation were plated onto 15cm NGM plates seeded with the 20X concentrated bacteria and grew to day 1. The worms were then harvested (day 1 sample) or filtered daily (filter out eggs and progenies) using a 40μm cell strainer and seeded onto a new 15cm NGM plate until day 5 before getting harvested (day 5 sample). Approximately 50k worms were used for day 5 sample collection and 100k worms were used for day 1 sample collection.

Germline mitochondria isolation was performed using methodologies described in Ahier et al. with modification.[74] In short, worms were harvested into a 15cm centrifuge tube and washed 3 times with 10ml M9 buffer and then 2 more times with cold KPBS buffer (136mM KCl, 10mM KH_2PO_4, pH = 7.2). The worms were then transferred to a dauncer on ice and daunced until most worms were clearly broken. Later, the lysates were transferred into a centrifuge tube for low-speed centrifugation to precipitate large fragments, and the supernatant containing the organelles was then collected and centrifuged again at high speed to precipitate the organelles. The pellet was resuspended in KPBS buffer, anti-HA magnetic beads (Pierce #88837) were added, and the tube was incubated at 4°C for an hour to ensure binding efficiency. The anti-HA magnetic beads were then washed three times with KPBS, portioned out for protein concentration measurement by BCA assay and mitochondrial DNA content detection by qPCR, and the remaining beads were stored at -80°C for later steps of GTP and ATP detection.

For detection of nucleotides, immunoprecipitated mitochondria (with around 100 to 200μg mitochondria protein) were resuspended in pre-chilled water to the concentration of 1μg mitochondria protein per μl water. 500μl pre-chilled chloroform was then immediately added to the resuspended mitochondria samples, followed by vigorous vortexing to quench metabolism and to extract soluble metabolites. The mitochondria extracts were centrifuged at 20000g for 10min at 4°C to remove the organic phase, followed by another centrifugation at 20000g for 10min at 4°C to remove cell debris. The resulting supernatants were diluted 10 times (to 0.1μg mitochondria protein per μl water) and analyzed immediately using HPLC-MS as described previously.[75,76]

Data analysis was performed using the Metabolomics Analysis and Visualization Engine (MAVEN) software.[77] For each sample, ion counts of nucleotides were normalized to mitochondrial protein mass followed by mtDNA level. All samples were then normalized to the (HT115 bacteria; D1) condition to indicate fold changes.

Cobalamin treatment

Methylcobalamin (Sigma-Aldrich #M9756) and adenosylcobalamin (Sigma-Aldrich #C0884) were administered to the *C. elegans* using methodologies similar to auxin treatment. A 1.28mM aqueous stock solution was freshly prepared and filtered through a 0.22μm filter. The stock solution was added into the NGM liquid agar with a concentration of 1 to 10000 (0.01%) after the autoclaved liquid agar dropped below 50°C and then poured into the plates making a final cobalamin concentration of 128nM. For the control plates, filtered double-distilled water was added to the NGM liquid agar instead. The plates were stored at 4°C inside a box with low photopermeability after the agar solidified. Bacteria were seeded before usage, and the plates that weren't used immediately were stored at 4°C for up to 5 days.

Succinate treatment

Sodium succinate (Sigma Aldrich #S2378) and succinic acid (Thermo Scientific Chemicals #AA3327236) were administered to the *C. elegans* via supplementation into the NGM plates. Precalculated amounts of sodium succinate and succinic acid were added into the liquid agar right after being taken out from the autoclave to make 10mM final concentration, and the agar was then poured into the plates after cooling down. The plates were stored at 4°C inside a box with low photopermeability after the agar solidified. Bacteria were seeded before usage.

Lifespan assay

Synchronized L1 larvae from egg preparation were plated onto 6cm NGM plates seeded with the bacteria that carry specific RNAi clones. Once reaching the L4 stage, worms were transferred to new 6cm plates, with 25-40 worms per plate and 80-120 worms per condition. Adult worms were transferred to new plates and examined every two days for their responses to gentle touch, to determine their status (alive or dead). The worms that could not be tracked until the day of death due to missing were counted as censors on the last day of valid observation.

QUANTIFICATION AND STATISTICAL ANALYSIS

The reproductive lifespan and lifespan analyses were performed using Kaplan-Meier survival analysis and a log-rank test in the SPSS. Chi-squared tests and Fisher's exact tests were performed in Graphpad PRISM to compare categorical variables, and Holm-Bonferroni method was used for correction as indicated in the corresponding figure legends. Student's t-test (unpaired) was performed in Excel to compare the mean of different samples, and Holm-Bonferroni method was used for correction as indicated in the corresponding figure legends. For all figure legends, asterisks indicate statistical significance as follows: n.s. = not significant $p>0.05$; * $p<0.05$; ** $p<0.01$; *** $p<0.001$. Data were collected from at least three independent biological replicates. Figures and graphs were constructed using BioRender, PRISM, and Illustrator.